Title
Helicon discharges and sources: A review*

Journal
Plasma Sources Science and Technology, 24(1)

ISSN
0963-0252

Author
Chen, FF

Publication Date
2015-02-01

DOI
10.1088/0963-0252/24/1/014001

Peer reviewed

IOP Publishing Plasma Sources Science and Technology

Plasma Sources Sci. Technol. **24** (2015) 014001 (25pp) doi:10.1088/0963-0252/24/1/014001

Helicon discharges and sources: a review*

Francis F Chen

Electrical Engineering Department, University of California, Los Angeles, CA 90095–1594, USA

E-mail: ffchen@ee.ucla.edu

Received 19 May 2014, revised 28 October 2014
Accepted for publication 3 November 2014
Published 20 January 2015

Abstract

Helicon waves are waves in low-temperature, partially ionized plasmas in a dc magnetic field (B-field). The study of helicons involves both ion–neutral collisions and Larmor orbits, even when the B-field is uniform. Helicon discharges are ionized by helicon waves generated by a radiofrequency (RF) antenna. Interest in helicon discharges arose because of the high plasma densities they generate compared with other RF sources at comparable powers. The semiconductor industry has not taken advantage of this, even since the possible use of permanent magnets for the B-field has been demonstrated. Nonetheless, a large literature on helicons has evolved because of the numerous problems these discharges posed and the interesting physics found in their solutions.

Keywords: helicons, helicon discharges, magnetized gas discharges, permanent-magnet helicons, helicon thrusters, discharge arrays, roll-to-roll processing

(Some figures may appear in colour only in the online journal)

1. A bit of history

In 1962 Peter Thonemann in the atomic energy laboratory at Harwell, UK, exclaimed, 'Take a look at this: an electromagnetic wave at a low frequency!' Indeed, Lehane and Thonemann [1] had produced what they thought was a pure electromagnetic wave at about 15 MHz, much lower than known electromagnetic waves in plasmas. . . say, electron plasma waves in the GHz range or electron cyclotron waves, also in the GHz range at 500 G (0.05 T). We now know that these 'helicon' waves are largely electrostatic, in spite of their excitation by an inductive antenna. The word *helicon* is the name of a mountain in Greece and of a river in Scotland. 'On the Banks of the Helicon' appears in the early music of Scotland. Here, helicon refers to the spiral nature of their waveforms and may have been chosen by Aigrain [2], who first studied these waves in semiconductors.

Among the early theorists were Leslie Woods [3, 4], Legendy [5, 6], Klozenberg *et al* [7], Bleven *et al* [8–10], Ferrari and Klozenberg [11], Davies and Christiansen [12] and Shoucri [13]. The Klozenberg paper gave the most complete treatment; however, since it predated the invention of personal computers, the calculations gave meaningless results. Many a helicon neophyte has labored over this paper. One of the students in England was Boswell, who made helicons his major field of interest. Moving back to Australia and finishing his studies in 1970, he made a small helicon discharge with a new type of antenna (now called a Boswell antenna), which could be clamped onto a discharge tube without opening the vacuum [14]. At the Australian National University he established an active group working on helicons. In 1985, Chen visited his laboratory during his sabbatical from UCLA. He became interested in helicons and brought the idea back to Shoji [15] in Japan and to R W Conn in the US. Conn and student G Campbell saw the possibilities and collaborated with Shoji to form the company PMT [16] to produce helicon sources for commercial use in semiconductor fabrication. An early application to plasma etching had been attempted by Chapman *et al* [17] in 1991. The MØRI source of PMT was made into a successful array that passed 'marathon' tests, but commercialization went no further. Since the early work cited above, helicons have become an active field, and over 2700 papers have been published on them [18]. Major contributors have been [18] Boswell *et al*, Scime *et al*, Shinohara *et al*, Chen *et al* and Shamrai *et al*. In addition, numerous researchers and groups in many countries throughout the world have joined in the effort to understand helicons.

Helicon waves have frequencies between the lower hybrid frequency $(\omega_c\Omega_c)^{1/2}$ and the ion plasma frequency Ω_p, and thus much lower than the electron cyclotron frequency ω_c.

* This article was originally part of the special 'Interaction of electromagnetic waves with low-temperature plasmas', published in PSST, vol 23, issue 6.

Initial studies therefore neglected the electron mass, though Boswell recognized that a second wave would exist when it was included [19]. This is now called the Trivelpiece–Gould (TG) mode. The first extensive papers describing helicons were published by Boswell [20] and by Chen [21, 22]. The coupled helicon (H) and TG modes are described by four coupled first-order differential equations [23]. A computational program, HELIC [24], for calculating the properties of H and TG waves, as well as for inductively coupled plasmas (ICPs) with no B-field, has been written by Arnush [23].

In recent years the 'double layer' created by a helicon discharge has attracted attention as a means of ion acceleration for spacecraft propulsion. C Charles [25] has written a review of this field. The dc B-field required by helicon discharges is cumbersome for both industrial and propulsion applications. This constraint can be relieved by the use of permanent magnets [26, 27]. Helicons are now widely known but have been put to practical use only in a few cases: for instance, in the fabrication of optical fibers [28] and in the propulsion of the Mars-bound spacecraft VASIMR [29].

2. Basic theory

Helicon waves are basically bounded whistler waves. Consider waves of the form $e^{i(m\theta+kz-\omega t)}$ propagating in a field $\mathrm{B} = B_0\hat{z}$. The dispersion relation for electromagnetic electron cyclotron R waves at an angle θ to $\boldsymbol{B}$ is

$$\frac{c^2\beta^2}{\omega^2} = 1 - \frac{\omega_\mathrm{p}^2/\omega^2}{1-(\omega_\mathrm{c}/\omega)\cos\theta} \underset{\omega_\mathrm{c}\gg\omega}{\rightarrow} \frac{\omega_p^2}{\omega\omega_\mathrm{c}\cos\theta} \tag{1}$$

Here β is the total k such that $\beta^2 = k_\perp^2 + k_z^2$. Defining $k \equiv k_z = \beta\cos\theta$, we have

$$\beta = \frac{\omega}{k}\frac{\omega_p^2}{\omega_\mathrm{c}c^2} = \frac{\omega}{k}\frac{n_0 e\mu_0}{B_0}. \tag{2}$$

This is the basic dispersion relation for helicon waves before we consider the complications. When the wave is confined to a cylinder of radius a, β is of order $1/a$, and equation (2) shows how the parallel phase velocity varies with density and magnetic field.

In a long cylinder, the boundary condition for waves with $ka \ll 1$ is [30]

$$m\beta J_m(k_\perp a) = 0. \tag{3}$$

Most experiments generate the lowest radial mode with an $m = 1$ antenna, so that $k_\perp a$ is the Bessel root 3.83. Since $k_\perp \approx b$, equation (2) gives

$$\frac{3.83}{a} \approx \frac{\omega}{k}\frac{n_0 e\mu_0}{B_0} \propto \frac{\omega}{k}\frac{n_0}{B_0}. \tag{4}$$

This shows that, for a given mode, the density should be proportional to B. We shall find that this occurs at high B-fields, but at fields below about 0.01 T there is a 'low-field peak' which violates this general condition.

3. The TG mode

When the electron mass is kept finite, a second wave is excited along with the helicon wave. This is an electrostatic electron cyclotron wave [31] localized near the radial boundary. Propagating at an angle to a magnetic field, this wave has been named the TG mode [32]. First found by Klozenberg [7] and by Boswell [33], the TG mode and its relation to the H-mode has been treated theoretically by Shamrai and Taranov [34], Borg and Boswell [35], Chen and Arnush [36], and numerous other authors. Combining Maxwell's equations with the electron equation of motion, they obtained

$$\delta\nabla\times\nabla\times\mathrm{B} - k\nabla\times\mathrm{B} + k_w^2\mathrm{B} = 0, \tag{5}$$

where $\delta = (\omega+\mathrm{i}\nu)/\omega_\mathrm{c}$, ν being the electron collision frequency with ions and neutrals, and

$$k_w^2 = \omega n_0\mu_0 e/B_0. \tag{6}$$

Equation (5) can be factored into

$$(\beta_1 - \nabla\times)(\beta_2 - \nabla\times)\mathrm{B} = 0, \tag{7}$$

where β_1 and β_2 are the roots of

$$\delta\beta^2 - k\beta + k_w^2 = 0. \tag{8}$$

These roots are, for $\delta k_w^2 \ll k^2$,

$$\beta_{1,2} = \frac{k}{2\delta}\left[1 \mp \left(1 - \frac{4\delta k_w^2}{k^2}\right)^{\frac{1}{2}}\right] \approx \frac{k}{2\delta}\left[1 \mp \left(1 - \frac{2\delta k_w^2}{k^2}\right)\right]$$
$$\approx \begin{cases} k_w^2/k \\ k/\delta. \end{cases} \tag{9}$$

The upper (−) sign gives the H-mode, and the lower (+) sign the TG mode. An example of this relation between k and β is shown in figure 1. Equation (6) shows that the curve depends on frequency, density, and B-field. The TG mode has large β and hence short radial wavelength. It is highly damped and therefore is localized near the boundary. The RF energy is often absorbed more by the TG mode than by the H-mode. Figure 2(a) shows the undamped radial profiles of the H and TG modes; these are greatly altered by damping. Figure 2(b) shows the radial deposition profile computed with HELIC for a sample case. The small peak at $r = 0$ due to the H-mode cannot be seen on this scale.

The presence of the TG mode has been seen in experiment [37]. It can be shown [37] that the TG mode affects the current profile $J(r)$ more than the field profile $B(r)$, and amplitude peaks at the edge due to the TG mode can be seen in figure 3.

4. Mode patterns

The electric field patterns for azimuthal wave numbers $m = \pm 1$ are shown in figures 4 and 5 [21]. The $m = -1$ mode has a much narrower profile, which may be the cause of its weaker propagation, as we shall see. The mode pattern for the $m = 0$ mode in figure 6 is entirely different: the wave changes from pure electrostatic to pure electromagnetic in each half-cycle.

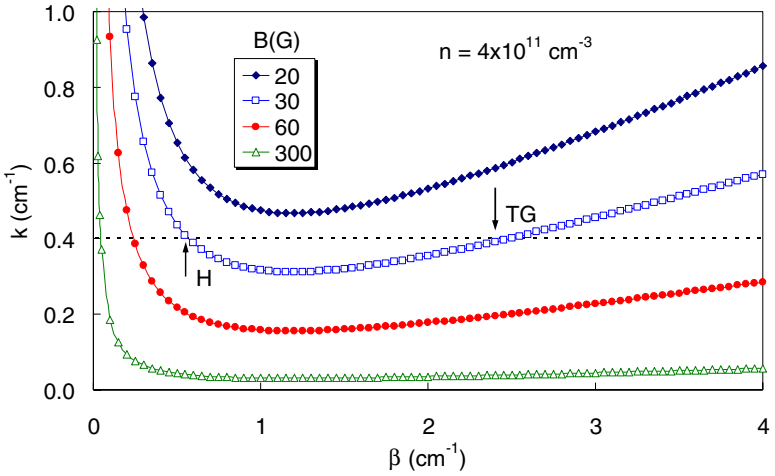

Figure 1. Example of the $k - \beta$ relation for coupled $m = +1$ helicon and TG waves at 11 MHz in a tube of 2.5 cm radius. Reprinted with permission from [36]. Copyright [1997], AIP Publishing LLC.

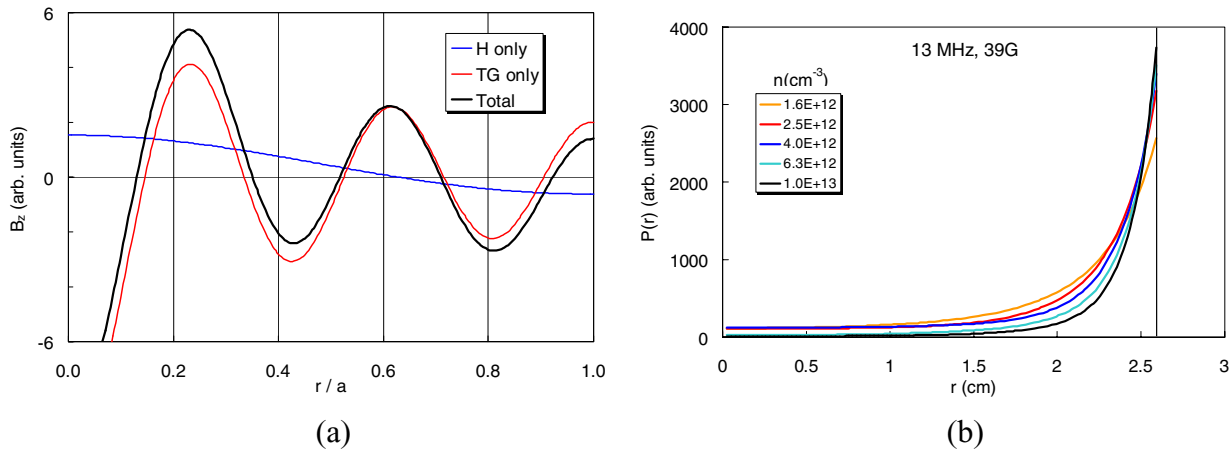

Figure 2. (*a*) Example of undamped $B_z(r)$ showing the H and TG modes separately (10^{12} cm^{-3}, 30 G, $m = 0$). (*b*) Example of an RF radial energy deposition profile showing the dominance of the TG mode.

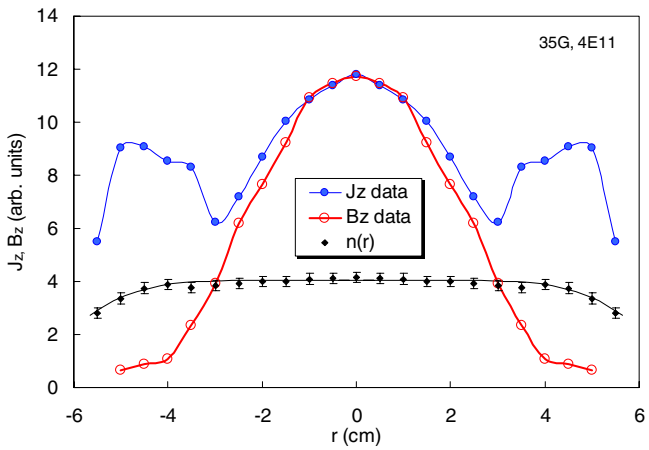

Figure 3. Profiles of $|B_z|$ (○), $|J_z|$ (●), and density measured in a helicon discharge 6 cm in radius and 110 cm long, with 1 kW of 11 MHz RF power in 2 mTorr of argon [37].

5. Antennas

In experiments on RF plugging of mirror machines, Watari *et al* [38] found that one type of antenna excited much larger RF fields in the plasma than the others. The reason for this was not known until the antenna was used in the Dawson separation process for purifying uranium using ion cyclotron waves. John Dawson's explanation, repeated here, had been published only in a book celebrating his 60th birthday [39]. Figure 7 shows a full-wavelength Nagoya type III antenna. Normally only half of this is used and is sufficient.

In a rising half-cycle, the RF current enters from the cable, splits in half at the center ring, and goes around the plasma to reach the top horizontal leg. There it splits again and goes left and right to the two end rings, where the current again goes around the plasma to reach ground via the bottom horizontal leg. Consider the top leg. As the current $\boldsymbol{J}$ rises, it generates a field $\boldsymbol{E}_m$ which opposes the rise. That field pushes electrons away from the center ring. Electrons then pile up near the end rings, leaving a positive space charge near the center ring. These charges generate an electrostatic field $\boldsymbol{E}_s$ pointing away from the center. The field $\boldsymbol{E}_s$ builds up until it stops the electron flow along $\boldsymbol{B}_0$. At the same time, the opposite currents and charges are created near the bottom leg. The antenna thus creates a pattern of space charges marked ⊕ and ⊖ on the diagram. These space charges in turn create a transverse E-field perpendicular to $\boldsymbol{B}_0$, as indicated by the heavy arrows. This vertical E-field is in the same direction as the $\boldsymbol{E}_m$ field of

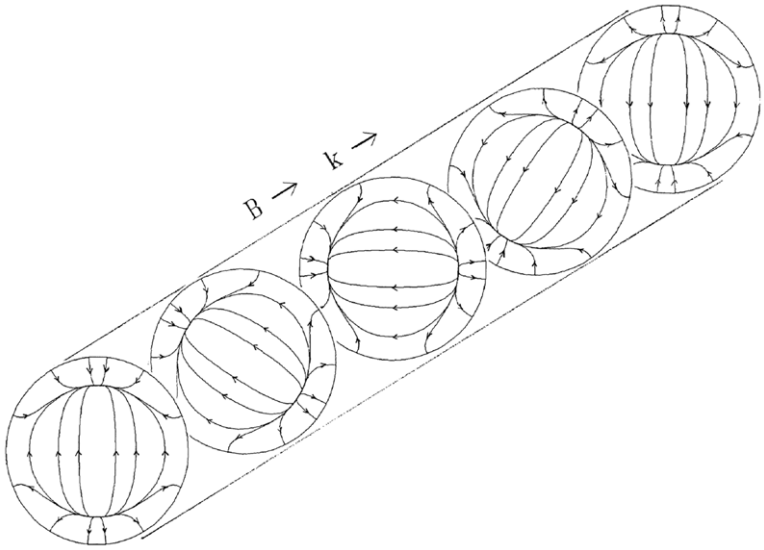

Figure 4. The $m = +1$ mode pattern rotates clockwise as seen by a stationary observer.

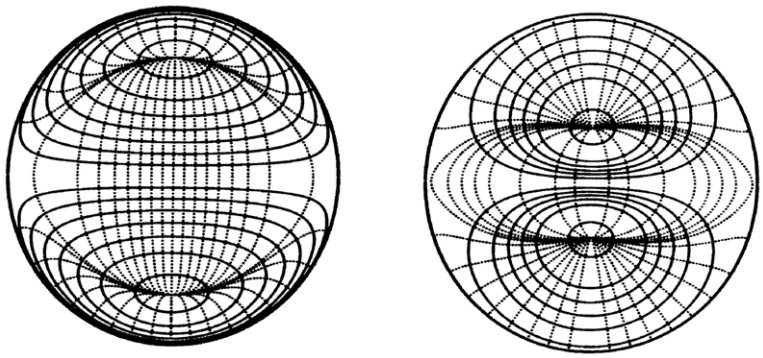

Figure 5. E-field patterns of the $m = +1$ (left) and $m = -1$ (right) modes.

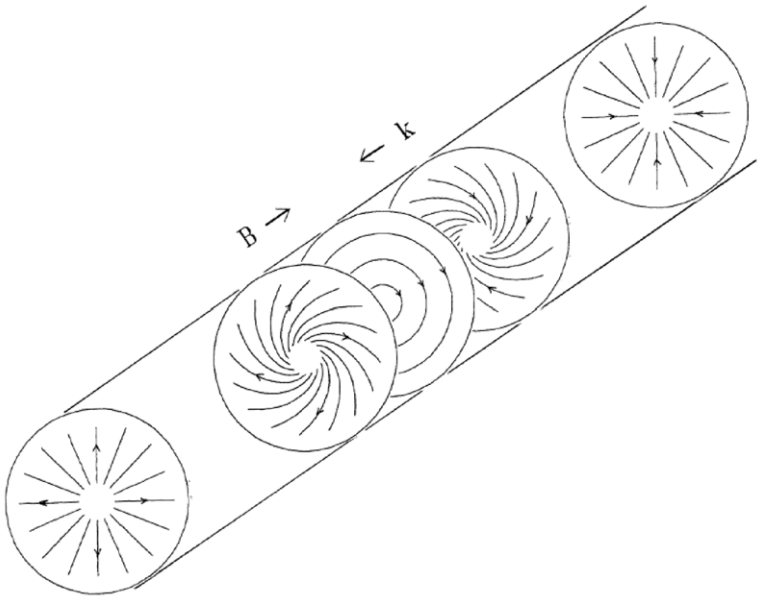

Figure 6. Mode patterns of the $m = 0$ helicon mode.

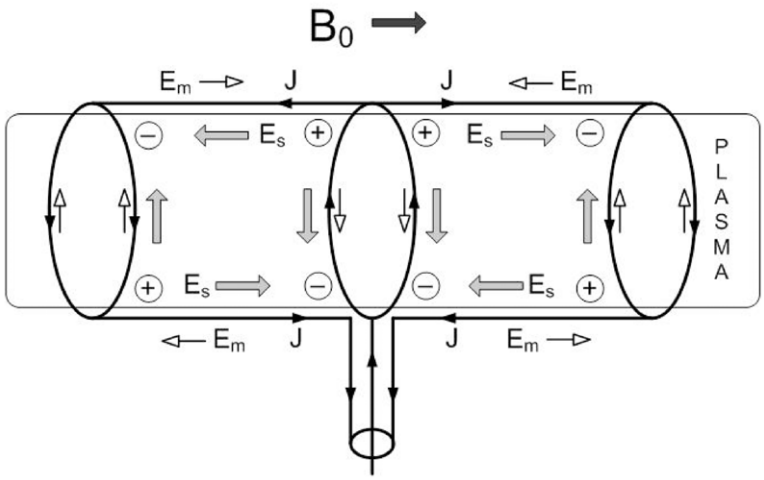

Figure 7. Diagram of a Nagoya type III antenna.

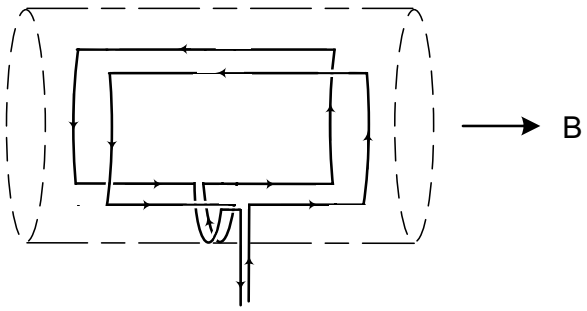

Figure 8. Schematic diagram of a Boswell antenna.

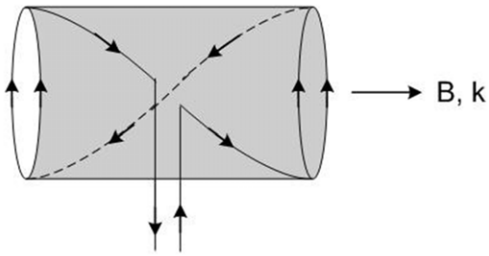

Figure 9. Schematic diagram of a half-wavelength right-helical antenna.

the ring currents but is much stronger, since the space charges have been collected over the length of the antenna. The longer the antenna, the larger the space charge must be to cancel the field $\boldsymbol{E}_m$. Hence, the antenna amplifies the applied RF field by creating electrostatic fields. It can be shown [40] with a rectilinear model of the antenna that the amplification factor is approximately $(k_\perp^2/k_\parallel^2)$, where the k are the antenna wavenumbers perpendicular and parallel to $\boldsymbol{B}_0$.

The Boswell antenna, shown in figure 8, is a modified Nagoya antenna with the top and bottom legs split into two wires so that the antenna consists of two separate halves. The advantage of this is that the antenna can be slipped around a cylindrical discharge tube without breaking the vacuum.

As shown by Miljak [41], helical antennas are Nagoya antennas twisted into right- or left-handed helices to better match the fields of the helicon wave. A 'right-helical' antenna, with azimuthal mode number $m = +1$, is shown in figure 9. This antenna creates much higher plasma densities than the left-helical $m = -1$ antenna, which is comparatively ineffective. The reason is not entirely clear, although the field patterns of the two are somewhat different (figure 5). The Nagoya antenna, being symmetric, generates both $m = +1$ and $m = -1$ fields, but the discharge is almost entirely due to the $m = +1$ mode.

In the $m = +1$ case, the same field pattern simply rotates as seen by a stationary observer (figure 4). The presence of electrostatic space charges can be seen from the convergence and divergence of the field lines at an intermediate radius. The azimuthally symmetric $m = 0$ helicon mode has an entirely different nature, as seen in figure 6. The E-field lines change from solenoidal (electromagnetic) to radial (electrostatic) in every half-cycle, with a mixture in between. Thus, the RF E-field there and the RF B-field are of equal importance. Such $m = 0$ antennas have been used commercially either singly or in pairs with currents in the same or opposite directions.

Matching the 50 Ω output of RF power supplies to the inductance of the antenna (the resistance of the plasma is small) is usually done with variable vacuum capacitors. The initial setting of these capacitors has to be close enough to ignite the discharge, after which the capacitors can be set to minimize the reflected power, done either manually or with an automatic tuning network. For given values of the antenna inductance and plasma resistance, the starting values of the capacitances can be found algebraically [42].

6. Landau damping

The phase velocities of helicon waves, as predicted by equation (4), can be comparable with electron thermal velocities, thus raising the possibility that electrons 'surfing' on these waves can be accelerated to ionizing energies, thus causing the helicons' high RF absorption efficiency [21]. This proposed mechanism was adopted by numerous

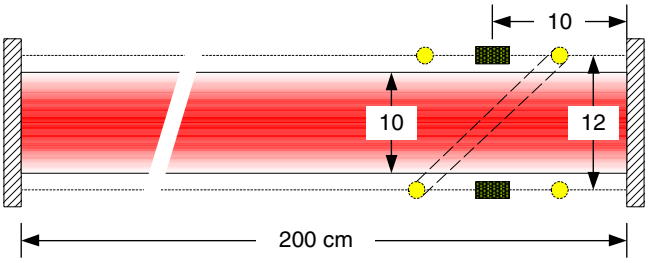

Figure 10. Geometry of the HELIC code. Here the assumed diameters of the plasma and the antenna, and the antenna position, are given in centimeters.

authors [43, 44] and was supported by detection of fast electrons by Ellingboe *et al* [45] using RF-modulated emission of Ar^+ light. However, Molvik *et al* [46] and Chen and Blackwell [47] showed with gridded energy analyzers that the number of fast electrons was insufficient to provide all the ionization in a helicon discharge. It was the TG mode described above that was the main ionization mechanism. Thus, the connection of helicons with Landau damping has turned out to be unimportant.

7. The HELIC code

After the invention of personal computers, numerous theorists devised codes for calculating helicon properties [48–51]. There have been many others, but the only code that has a user interface and is open-source [52] is the HELIC program by Arnush [23], which solves the following coupled first-order differential equations:

$$\frac{\partial E_\varphi}{\partial r} = \frac{\mathrm{i}m}{r}E_r - \frac{E_\varphi}{r} + \mathrm{i}\omega B_z$$
$$\frac{\partial E_z}{\partial r} = \mathrm{i}kE_r - \mathrm{i}\omega B_\varphi$$
$$\mathrm{i}\frac{\partial B_\varphi}{\partial r} = \frac{m}{r}\frac{k}{\omega}E_\varphi - \frac{\mathrm{i}B_\varphi}{r} + \left(P - \frac{m^2}{k_0^2 r^2}\right)\frac{\omega}{c^2}E_z$$
$$\mathrm{i}\frac{\partial B_z}{\partial r} = -\frac{\omega}{c^2}\mathrm{i}DE_r + \left(k^2 - k_0^2 S\right)\frac{E_\varphi}{\omega} + \frac{m}{r}\frac{k}{\omega}E_z. \qquad (10)$$

These equations follow from Maxwell's equations and the cold-plasma equations with the familiar S, P, D dielectric elements [53]. They are derived in three papers by Arnush [23, 36, 54]. HELIC solves these equations for each k of the antenna spectrum, and for each value of n and B_0. A typical run for $R(n, B)$, as in figure 14 later, takes about 1–2 h on a personal computer. Figure 10 shows the geometry used for the HELIC code. The antenna can be any of the common types and can be located at any distance from one endplate. The endplate separation can be specified. The assumed plasma can vary radially but not axially. For short discharges, the assumed radial profile can be calculated from a recent theory [50].

Figure 11 shows the input and output pages of the HELIC desktop. The inputs include (1) the discharge and antenna radii, the discharge gas and frequency, the antenna type and distance from an endplate, (2) the ranges of density and B-field to be calculated, either linearly or logarithmically spaced, and the radial density, temperature, and pressure profiles, and (3) some calculational choices. The outputs include the power spectrum of the antenna, the radial and axial deposition profiles, all the wave fields versus r and z, and, most importantly, $R(nB)$, which is the plasma resistance versus n and B_0. This quantity should be at least 1 Ω for the RF power to be deposited mostly in the plasma rather than in the circuitry. The wave fields can be obtained with the H and TG parts separated. At high B-fields, these modes merge and cannot easily be identified. A high-field formulation of the equations has then to be used, and Arnush has provided an adjustable point for transition to the high-field case.

Figure 12 is an example of a plot of $P(r)$, the radial power deposition profile. Note the transition from H-mode to TG-mode deposition as the density is increased. Figure 13 is an example of the axial power profile $P(z)$. We see that much of the power is deposited downstream of the antenna. There is also a small peak at the endplate, where the wave is reflected. Figure 14 is a plot of $R(n)$ for various B_0 showing peaks in R. These are the low-field peaks to be discussed later. The plasma losses are proportional to n and can be represented by a straight line. The operation point is the intersection of this line with the right-hand side of one of the curves. This is the stable point [55], since the loading increases with a decrease in n, and vice versa. Such curves are used only as guides for the design of an experiment.

The HELIC code made it possible to design the diameters and lengths of helicon discharges for operation at various magnetic fields and densities, as long as n, B and T_e are uniform in the direction of $\boldsymbol{B}$. Similar curves have been obtained by Suwon Cho *et al* [56–59].

8. The low-field peak

In early experiments on helicons [60], it was observed that when the field lines terminated on the glass tube, as shown in figure 15, the discharge was effectively bounded by an insulating endplate. The density was then increased over the case of a uniform field (figure 16). In the same device, it was found that n did not increase monotonically with B_0, as predicted by equation (2), but had a small peak (figure 17) at low fields of the order of 60 G (0.006 T). This low-field peak [61, 62] could also be produced with a conducting endplate, as shown in figure 18. In either case, the explanation is that the helicon wave is reflected constructively from the end boundary (with opposite phases for conductors and insulators), thus increasing the ionization and the density. This mechanism is illustrated in figure 18. To confirm this, HELIC computations were carried out for unidirectional and bidirectional antennas, as shown in figure 19. The peak occurs strongly for simple loop antennas, which are bidirectional. The low-field peak has also been seen by Sato *et al* [63] and explained by Cho [64]. This effect will be used in compact permanent-magnet helicon sources described later.

9. Early experiments

This review of experiments does not differentiate between pulsed and steady-state discharges. To limit the heating

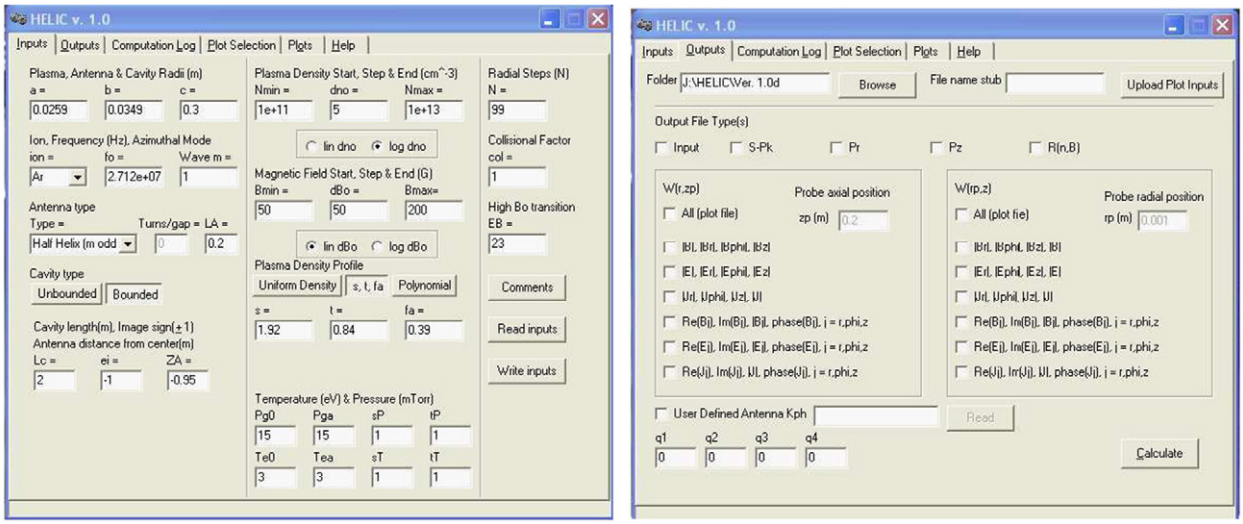

Figure 11. The input page (left) and output page (right) of the HELIC program.

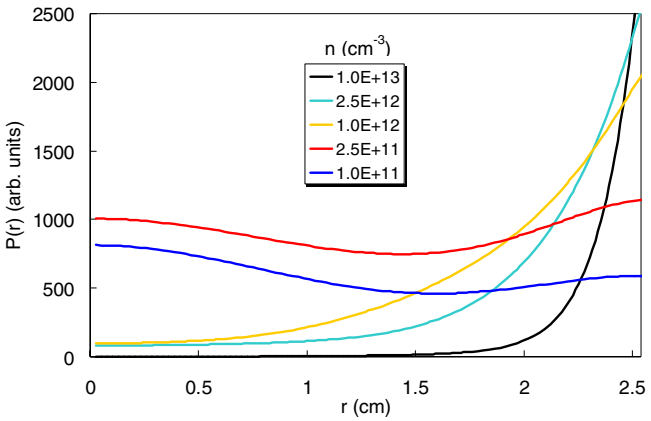

Figure 12. Example of a HELIC calculation for radial power deposition profile in a single-ended cylinder of 2.5 cm radius. The 50 G (0.005 T) discharge is at 27.12 MHz in 15 mTorr of argon. The $m = 0$ antenna of 3.49 cm radius is 5 cm from the endplate. KT_e is assumed uniform at 3 eV, but the density has a 'universal' profile [50]. The legend refers to the curves from top to bottom at the extreme right.

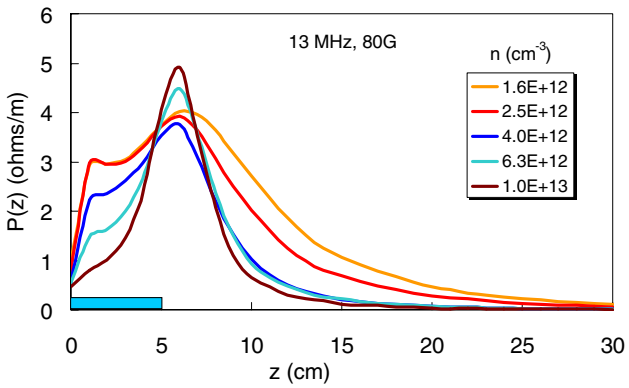

Figure 13. Example of a HELIC calculation of axial power deposition profile in the tube specified in figure 11, but at 13.56 MHz and 80 G (0.008 T). The legend lists the curves in the order of peak height (not uniform). The location of the tube is shown at the bottom.

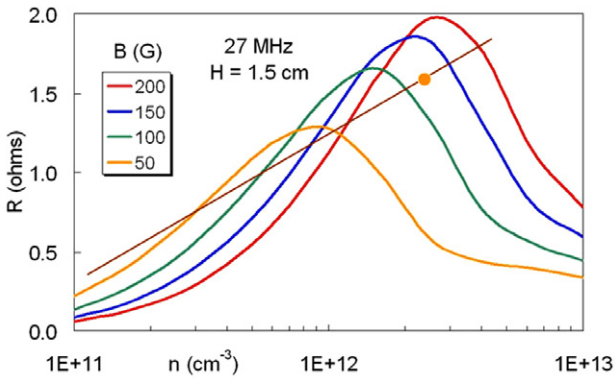

Figure 14. Example of $R(n, B)$ curves calculated by HELIC for a 5.1 cm diameter tube with an $m = 0$ antenna 1.5 cm from the endplate. The energy losses are represented by the straight line. The dot shows an operating point at $n \approx 10^{12}$ cm^{-3}.

of probes and O-rings, the RF is often pulsed for 10–1000 ms, during which the plasma reaches equilibrium and measurements can be made. In steady-state operation, the neutral density can also reach its equilibrium profile. Fast probes have been made in the past to sample dense dc discharges.

The first large helicon discharge was built by Boswell in Australia. The BASIL machine [65], 4.5 cm in diameter and 160 cm long, had B_0 up to 1600 G (0.16 T) and RF power (P_{rf}) up to 5 kW at 7 MHz. Running at 1 Pa of argon, it achieved a peak density of 10^{20} m^{-3}. A second machine, the WOMBAT [20], shown in figure 20, had a helicon source 18 cm in diameter and 50 cm long, injecting the plasma into a large chamber 90 cm in diameter and 200 m long. As power or B-field is increased, an RF discharge changes from a capacitive to an inductive to a helicon discharge, as shown by Degeling *et al* [66]. The transition into a helicon discharge as the RF power is increased was shown by Chi *et al* [67] and by Ellingboe *et al* [68] As seen in figure 21(a), the RF at low power is capacitively coupled to the plasma via the voltage on the antenna.At higher power it is the RF magnetic field which

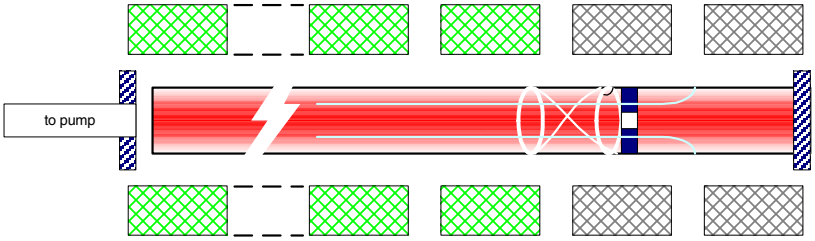

Figure 15. A helicon discharge ending on an insulator or a conducting endplate (not at the same time). The cusped field is formed by turning off the two end coils.

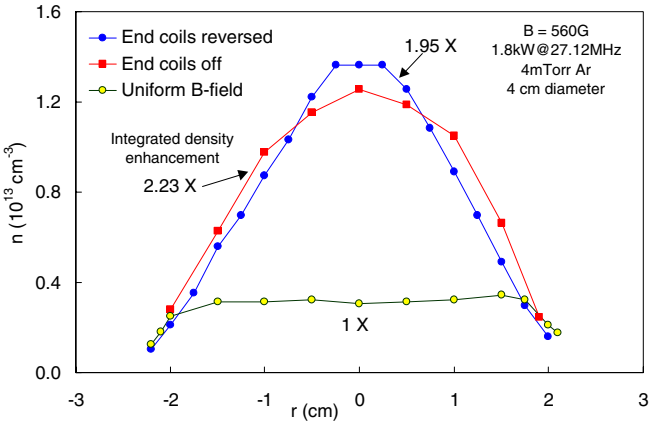

Figure 16. Density enhancement with magnetic cusps at the ends of the discharge; data from [70].

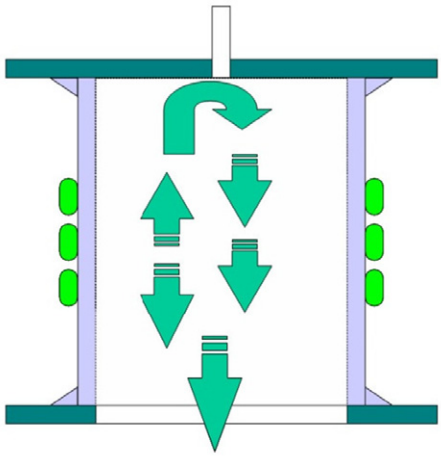

Figure 18. Mechanism of the low-field peak.

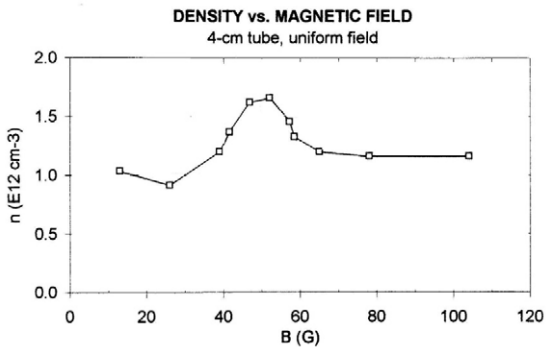

Figure 17. A low-field density peak Reproduced with permission from [60]. Copyright [1992], American Vaccum Society.

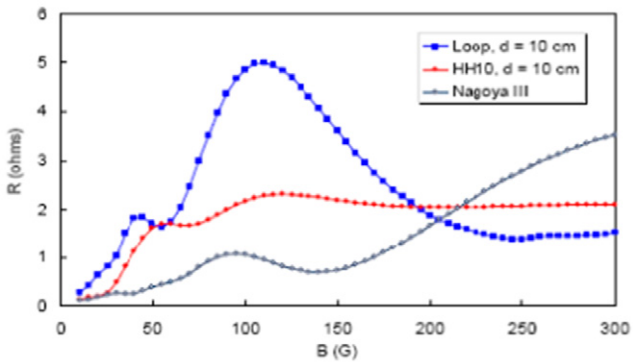

Figure 19. HELIC calculations of $R(B_0)$ for bidirectional and unidirectional (HH10, helical) antennas.

excites currents in the plasma after the gas breaks down from the E-field. Finally, the power is high enough to generate a density matching the helicon conditions. Jumps can also be seen at constant B-field and increasing power, as seen in figure 21(b) [20]; in this case, the jumps are from one helicon mode to another. An alternative explanation of jumps was later suggested by Chen and Torreblanca [69]. A jump can occur when the plasma resistance R exceeds the circuit resistance. This was verified in their experiment.

After bringing the helicon idea to the US, Chen built the linear experiment shown in figure 22. The coils were mounted as received from the factory without rewinding, leaving gaps for probes. The original matching circuit used waveguides with sliding stubs; vacuum capacitor units were available later. The coils and the RF were pulsed for less than 100 ms, thus avoiding water cooling. These early experiments [70] tested the Nagoya and helical antennas and the effect of cusp fields at the endplate. The antenna studies by Miljak [41] were also carried out on this machine.

A larger machine (not shown), with a 10 cm diameter tube 108 cm long, with pulsed fields up to 0.1 T, was built by Blackwell [71]. Figure 23 shows end views of the discharge in 488 nm Ar^+ light. In (a), the discharge is just above the jump from capacitive to inductive coupling and shows the location of the antenna bars at top and bottom. After addition of a Faraday shield in (b), the discharge is more symmetric with the removal of the antenna's E-field. In (c), a helical antenna produces a dense, symmetric plasma. This is seen as a narrow, bright blue column, even in smaller 5 cm diameter discharges, and has been named the Big Blue Mode. We surmise that it occurs

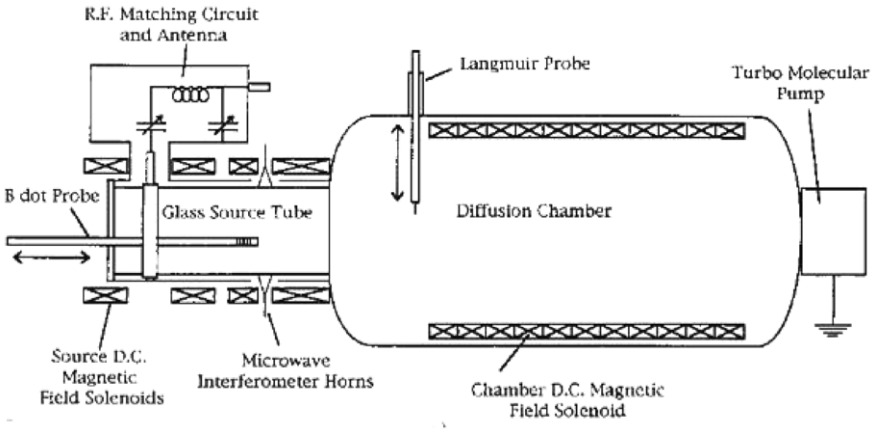

Figure 20. The Australian WOMBAT machine. Reprinted with permission from [66].

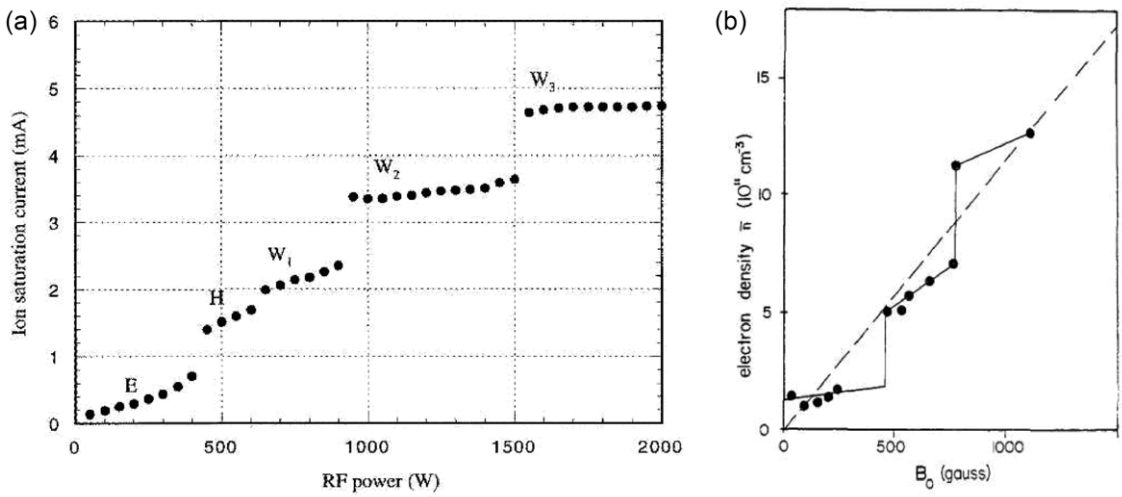

Figure 21. (*a*) Density jumps versus RF power [67]. (*b*) Mode jumps versus B_0 [20].

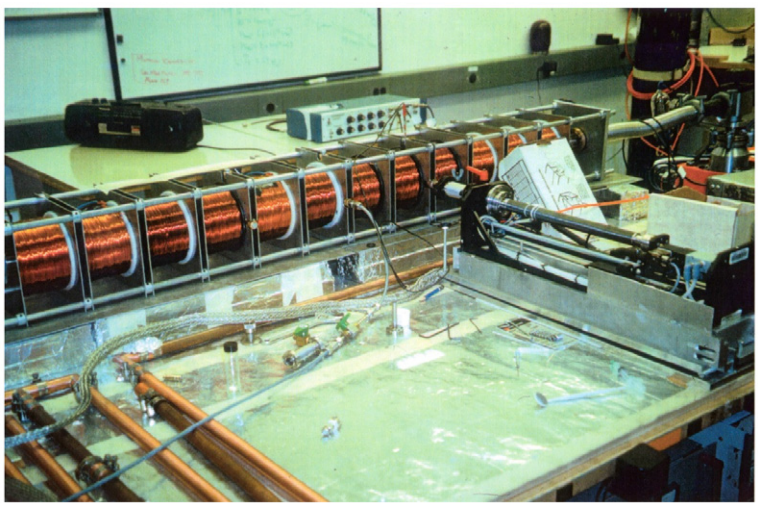

Figure 22. The first helicon experiment in the US.

because of an ionization instability: as neutrals are depleted, electrons make fewer collisions, and KT_e rises. This increases the ionization rate exponentially. The asymmetry seen in (*c*) is caused by a Langmuir probe.

A side view of this discharge in figure 24, taken at three ports, shows the difference between $m = +1$ and $m = -1$ helical antennas. Though the light intensity differences are not clear in these early data, the $m = -1$ antenna generates a

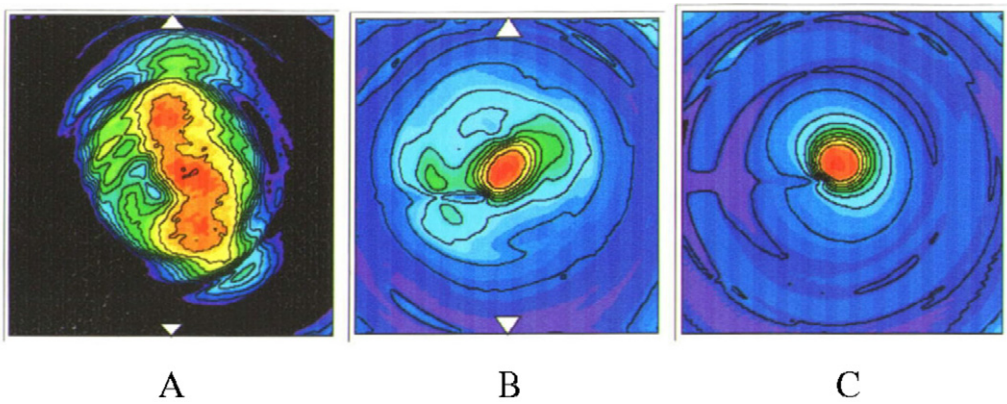

Figure 23. End views of a helicon discharge with (*a*) a straight Nagoya III antenna with no Faraday shield, (*b*) the same antenna with a Faraday shield and (*c*) a right-helical antenna with or without shield [71].

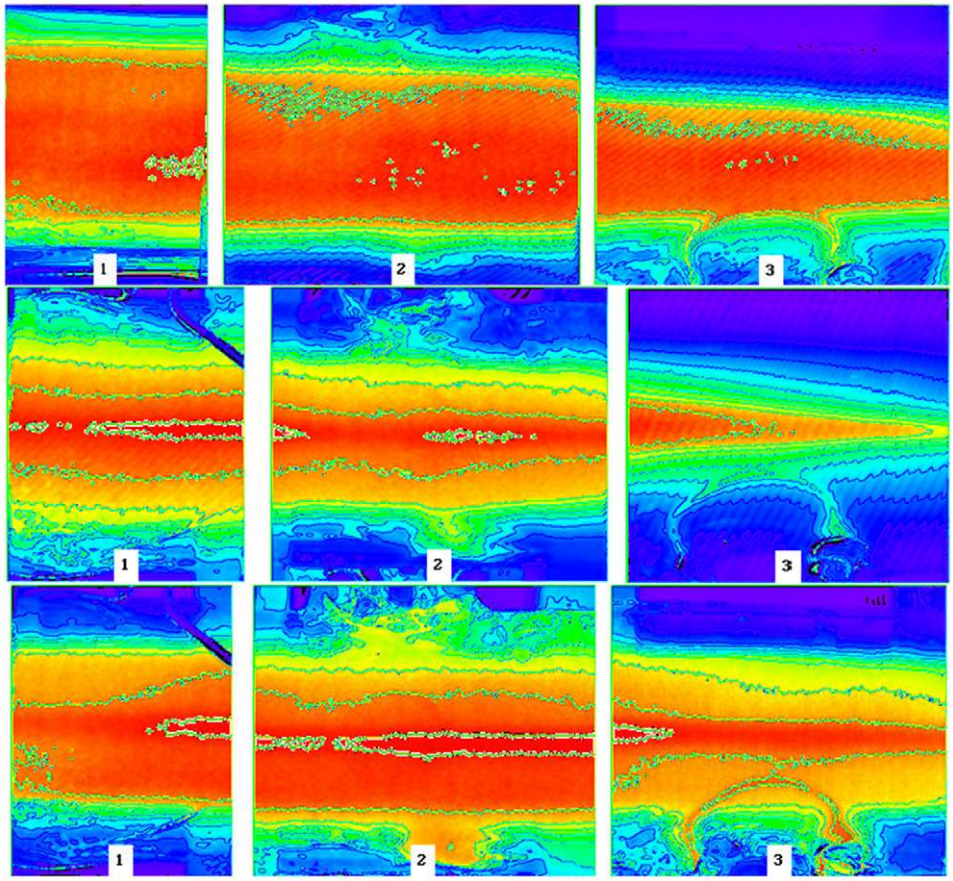

Figure 24. Side views of a 10 cm diameter helicon discharge. The top row is for a Nagoya type III, the second row is for an $m = -1$ helical, and the bottom is for an $m = +1$ helical antenna [71].

low-density plasma that fades axially. The $m = +1$ antenna gives a long, dense plasma. The straight, bidirectional Nagoya antenna gives a less dense plasma that also reaches the end of the tube.

An experimental check of theory for radial B_z profiles was performed by M Light [72] using a loop probe. Shown in figure 25 are measured and computed profiles for the case $\boldsymbol{k}||\boldsymbol{B}_0$ with a right-helical antenna. The measurements agree reasonably well with the theory for an $m = +1$ mode but not for an $m = -1$ mode. Axial profiles of the wave fields are shown in figure 26 [64]. The wave amplitude oscillates downstream from the antenna. This was found to be compatible with the expected beating of two modes with different values of k, as shown by the theoretical curve.

10. More recent experiments

After these initial forays, research into helicons expanded worldwide. Samples of the experimental efforts follow.

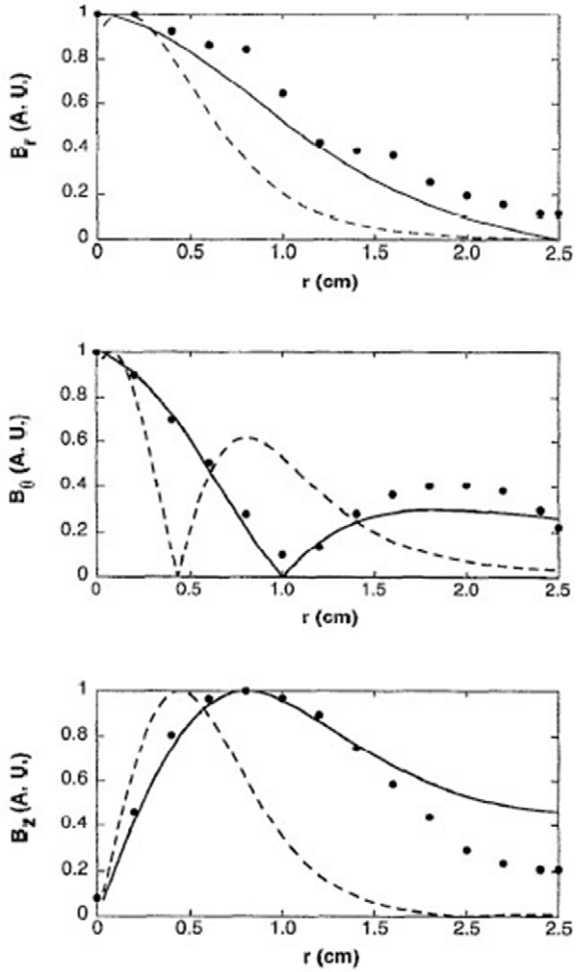

Figure 25. Example of comparison of experiment (dots) with theory (lines) for $B_z(r)$. The solid line is for the $m = +1$ mode, and the dashed line for the $m = -1$ mode [72]. Reproduced with permission from *Phys. Plasmas* **2** 1084, Copyright 1995, AIP Publishing LLC.

10.1. Experiments by Shinohara et al

A large helicon machine was built in Japan by Shinohara *et al* [74, 75] It is shown in figure 27. Properties of the plasma have been studied with changes in the B-field uniformity and endplate conductivity [76], different types of antenna [77], including flat spirals tapped at various points and arrays of $m = 0$ loop antennas [78–80], and different sizes and aspect ratios of the discharge column, including diameters as small as 1 cm [81]. By biasing concentric-ring antennas, the radial electric field and plasma profile can be changed to study instabilities [82–84]. The extensive studies of helicons under disparate conditions by Shinohara and collaborators have demonstrated the versatility of helicons for various applications.

10.2. Experiments by Scime et al

Earl Scime has probably been the most active promoter and researcher in helicon physics. The breadth of activity on helicons can be seen in his summary [85] of papers presented in a mini-conference that he organized at the 2007 meeting of the APS Division of Plasma Physics. In his own group

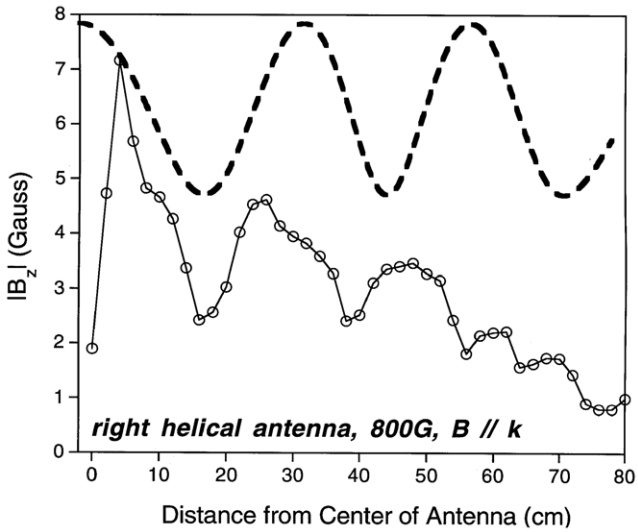

Figure 26. Example of comparison of experiment (dots) with theory (dashed lines) for $B_z(z)$ [73]. Reproduced with permission from *Phys. Plasmas* **2** 4094, Copyright 1995, AIP Publishing, LLC.

at West Virginia University, experiments are mostly done on the HELIX machine [86], shown in figure 28. The antenna is on a 10 cm diameter Pyrex tube leading into a 15 cm diameter metal chamber, and then into the large expansion chamber. A distinguishing feature of this experiment is the laser induced fluorescence (LIF) system, which can measure the perpendicular ion temperature. This was found to be much higher than expected from equilibration with neutral atoms [86, 87], indicating a source of ion heating. This source was conjectured to be a parametric decay instability in which the RF generated a lower hybrid wave and an ion acoustic wave, and the latter was the ion heating mechanism [88] (figure 29).

A recent experiment in this group had two special features. First, it was done in krypton, an expensive gas that is rarely available. Second, a new diagnostic, two-photon absorption laser induced fluorescence, was developed to measure the neutral density profile. One result was the finding that, as the B-field was increased from 600 to 1200 G, with power increasing from 600 W at 13 MHz to 800 W at 11 MHz, the plasma changed from a gently peaked profile with uniform neutral density to a sharply peaked profile with total neutral depletion on axis. This helps to justify the conjectured explanation for the big blue mode mentioned in section 9.

10.3. Experiment by Krämer et al

Deposition of RF energy from the TG mode into the plasma was found by Krämer *et al* [89, 90] to involve an interesting process involving parametric instabilities. Figure 30 plots the electrostatic field from a capacitive probe, showing sidebands arising from the low-frequency oscillation seen at the left. These ion acoustic waves are created by parametric decay of the helicon wave via the process shown in figure 31. The ion waves were shown to grow nonlinearly with RF power. Though the phases and other details of the parametric interaction were measured in detail, it is not clear whether this process is important in the transfer of RF energy into

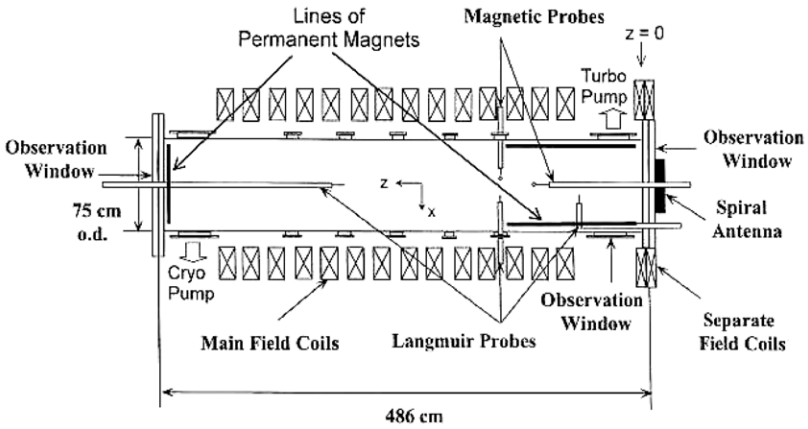

Figure 27. A large helicon machine (courtesy of Shinohara).

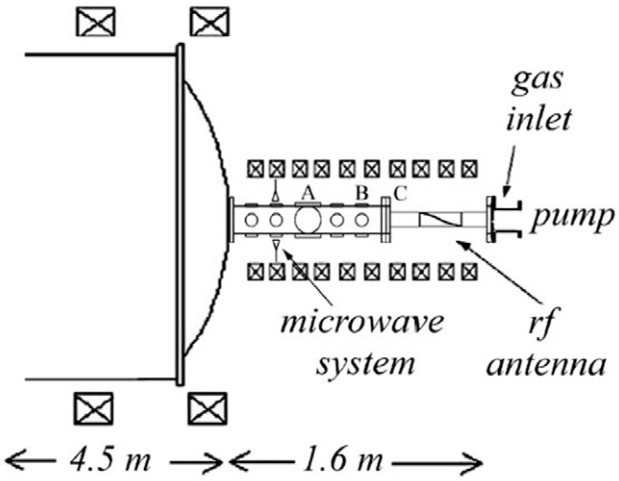

Figure 28. The HELIX helicon source at West Virginia University [86].

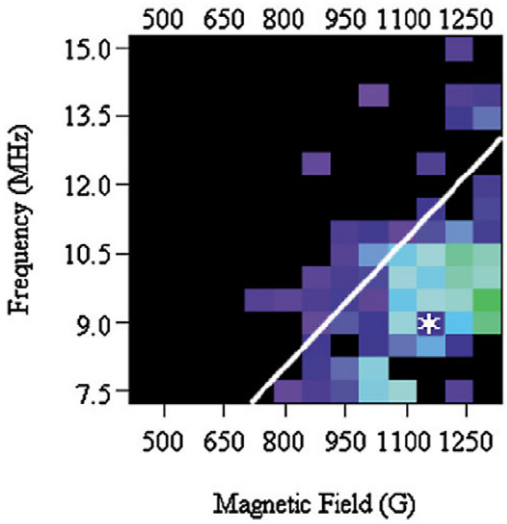

Figure 29. Evidence of high ion temperatures below the lower hybrid frequency (line) [87].

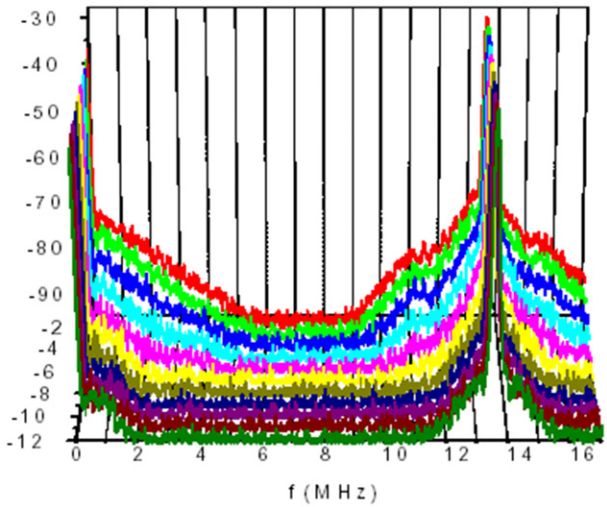

Figure 30. Electrostatic field of the TG mode and its decay into ion waves, as RF power is raised [90].

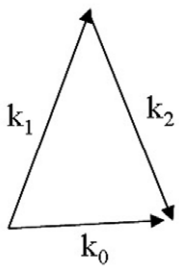

$$\omega_0 = \omega_1 + \omega_2$$
$$\mathbf{k}_0 = \mathbf{k}_1 + \mathbf{k}_2$$
$$\mathbf{k}_{\perp 0} = \mathbf{k}_{\perp 1} + \mathbf{k}_{\perp 2} \approx 0, \quad \mathbf{k}_{\perp 1} \approx -\mathbf{k}_{\perp 2}$$

Figure 31. Decay scheme of figure 30. k_0 is the helicon wave, and k_1 and k_2 are the TG wave and an ion acoustic wave.

the plasma. Calculations for this experiment were carried out by Fischer [91]. Incidentally, this experiment used a vertical helicon discharge, in which the magnetic coils were stacked vertically, greatly simplifying the coil mounts.

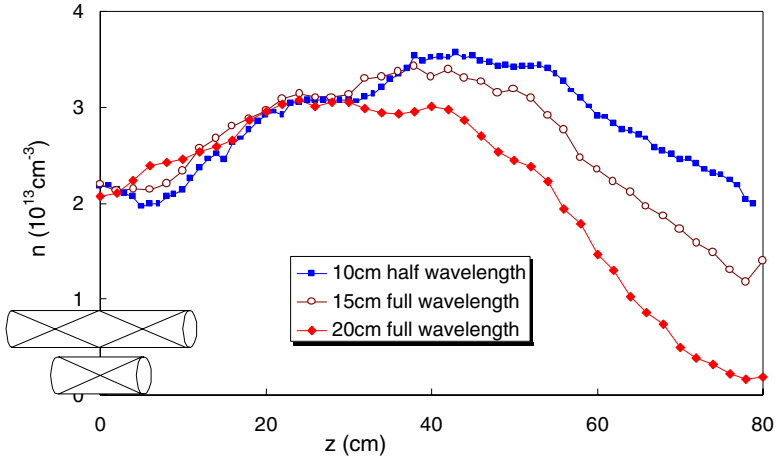

Figure 32. Density profiles $n(z)$ with full- and half-wavelength helical antennas centered at $z = 0$ [130].

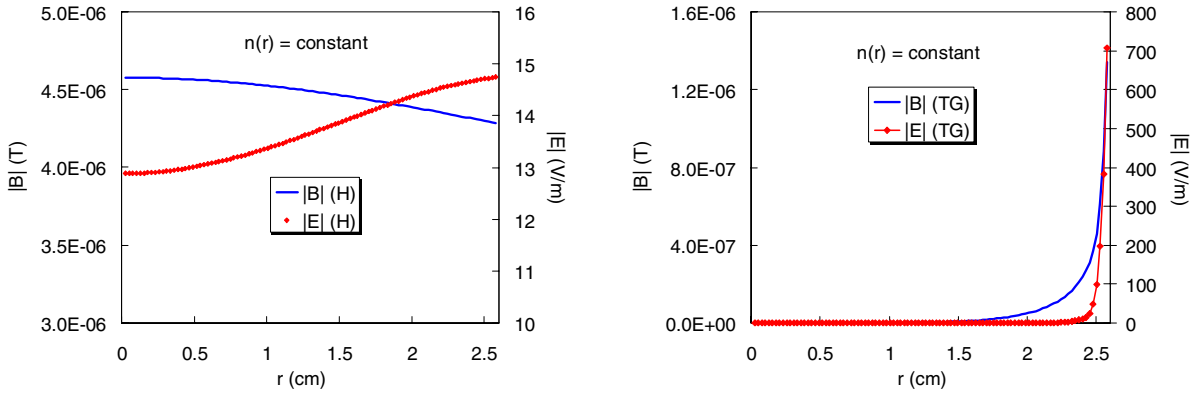

Figure 33. Computed $|B|(r)$ and $|E|(r)$ for the H and TG modes in a uniform plasma with $B_0 = 0.1$ T at 13.56 MHz, $n(0) = 10^{12}$ cm^{-3}, $KT_e = 3$ eV, $p = 15$ mTorr of argon, and an $m = 1$ half-helical antenna carrying 1 A of current. Note the suppressed zeros.

10.4. Experiments by others

Helicon experiments have been done all over the world. Only a sampling can be given here. In Japan, Sakawa *et al*, working with T. Shoji [15] and others, studied helicon production with $m = 0$ loops [92–94]. This work eventually led to the commercial MØRI machine in section 13. As shown in figure 6, the $m = 0$ mode has a completely different structure from the asymmetric modes. Also from Japan, the work by Shinohara was covered above. Y. Mori *et al* [95] successfully excited helicons in hydrogen both above and below the lower hybrid frequency. They also saw a low-field peak (section 8).

In Korea, Yun, Kim, and Chang have studied helicons near the lower hybrid frequency [96], excited the $m = \pm 1$ and ± 2 modes [97], and measured the ionization efficiency of helicons [98]. Yun *et al* have found a density rise near the LH frequency with $m = 0$ antennas [99]. Kim and Chang measured the ion energy distributions [100], and Eom *et al* [101–103] have generated helicons at high frequencies up to 180 MHz.

In Australia, helicons were also used to create the plasma in toroidal fusion experiments [104, 105]. A new large helicon source, MAGPIE, has been built at ANU, and Chang *et al* [106] have separately controlled and measured the radial and axial profiles of the plasma and the waves.

In Germany, a large helicon machine, VINETA [107], was built at Greifswald. It had four identical modules, each with eight large magnet coils. Detailed profiles of the plasma and the wave properties were obtained in both helicon and capacitive modes.

In France, Corr *et al* observed ion acoustic waves as sidebands of the RF frequency [108] and created stable helicon discharges in Ar/SF_6 mixtures [109]. Further, in connection with plasma processing, Petri *et al* [110] measured the oxygen from the walls in an SF_6 helicon plasma.

In India, helicons have caught the interest of many physicists. Sahu *et al* [111, 112] showed that this interest had reached beyond the major institutes. Ganguli *et al* [113] calculated the helicon wave fields, with damping, for various levels above the minimum of a curve in figure 1. The double layer which they observed [114] in experiment is a more gentle potential drop than is seen by others. Paul and Bora [115] used helicons for RF current drive in a torus. The new twist is that the current is driven nonresonantly via helicity injection. Anitha *et al* [116] studied the trapping of helicons in a magnetic bubble, a mirror trap with $B \approx 0$ at the center. Tarey *et al* [117] built a helicon source 15 cm in diameter and 160 cm long, in which they studied axial particle confinement with magnetic mirrors and electric barriers. Barada *et al* [118] observed low-field helicons near electron cyclotron frequency

in a 10 cm diameter chamber with a helical $m = +1$ antenna at the center. The electron cyclotron peak at 5 G was observed on the 'backward' side of the antenna but was very small on the 'forward' side.

In the US, the large helicon machine of N Hershkowitz, shown later in figure 34, was the centerpiece of the Wisconsin NSF Center for Plasma Aided Manufacturing. Among the many papers from this program are a study of neutral pumping by the helicon plasma [119] and observation of electron beams accelerated by the waves [120]. In the EECS Department at Wisconsin, John Scharer's group built a 10 cm diameter, 122 cm long helicon source [121] and measured the plasma and wave profiles in both uniform and nonuniform B-fields. A major contribution was a 2D code for helicons, similar to the HELIC code [23], written by Mouzouris [122]. At the University of Illinois, Urbana, Reilly and Miley [123] have used magnetic probes to see the three-dimensional structure of a helicon wave. They found deviations from the azimuthal symmetries that are usually assumed.

At the University of California San Diego, G Tynan has constructed the large machine CDCX [124] (Controlled Shear Decorrelation Experiment) to simplify instability and transport effects in tokamaks to linear geometry. The helicon source is 10 cm in diameter, with a two-loop $m = 0$ antenna driven up to 1500 W at 13.56 MHz, and injects plasma into a 3 m long chamber with a field of 1000 G. At the far end, a series of concentric rings is used to measure the radial plasma transport. The plasma is subject to drift-wave instabilities peaking at 3 cm radius at a frequency of ~25 kHz. The plasma turbulence is characterized with correlation measurements, leading to a turbulent Reynolds stress $\langle(\mathrm{d}/\mathrm{d}r)(\tilde{v}_r\tilde{v}_\theta)\rangle$. According to P Diamond [125], this should drive a poloidal flow, which was indeed seen and measured [126]. In collaboration with Scime (see section 10), laser induced fluorescence was brought to the experiment, and this sheared poloidal flow was directly measured, along with the perpendicular ion temperature [127]. This brief summary cannot do justice to the sophistication of this experiment.

On the theoretical side, recent contributions from the US include the possibility of very low-frequency helicons in radially localized modes predicted by Breizman and Arefiev [128], and a detailed treatment of charge exchange collisions with realistic ion orbits by the same authors [129].

11. Conundrums and insights

Throughout the history of helicons numerous problems have arisen in the behavior of these discharges. As one mystery was solved, another would appear. It is like the peeling of an onion: each layer reveals another one underneath. Here we shall describe some of these layers.

(1) Why does the amplitude oscillate along the cylinder?
The solution was given in the previous section: it is due to the beating of simultaneous excitation of waves with two values of k.

(2) Why is a right-helical antenna better than a left-helical one?
HELIC calculations show a higher value of plasma resistance R for the $m = +1$ mode than for the $m = -1$ mode. If by right-helical antenna we mean one that launches an $m = +1$ mode in the 'downstream' direction away from an endplate, this is expected since the mode patterns of figure 5 show stronger fields at the edge for the +1 mode.

(3) What causes the high ionization efficiency?
This was found to be due partly to the TG mode, whose fields are necessary to satisfy the boundary conditions at the confining radial wall.

(4) Why does an endplate behind the antenna increase n?
This is caused by the reflected wave, as shown in figure 18.

(5) Why is the density peaked at the center?
The density has to decrease radially so that Maxwellian electrons can create an E-field pointing outward, pushing the ions out. If the density were low on the axis, ions would be pushed inward by the E-field and could only escape to the endplates at their slow thermal speeds. The central density would then build up until it is highest there.

(6) Why is the ion temperature so high?
E Scime *et al* have contributed extensively to the science of helicons. One of their discoveries is that the ion temperature is much higher than would be expected from thermal equilibrium with the neutral gas. This was attributed to ion Landau damping at the lower-hybrid frequency.

(7) Why is a half-wavelength antenna better than a full-wavelength one?
It would seem reasonable that a full-wavelength helical antenna would have a narrower spectrum and would couple better to the plasma than the usual half-wavelength antenna. But it was found [130] (figure 32) that the opposite is true. This has not yet been explained.

(8) Why is the discharge sometimes hard to ignite?
When an RF pulse is applied to the antenna, a few electrons from the cosmic ray background are accelerated, strike neutral atoms, and cause an avalanche, which starts the ionization process. At low pressures and small diameters,

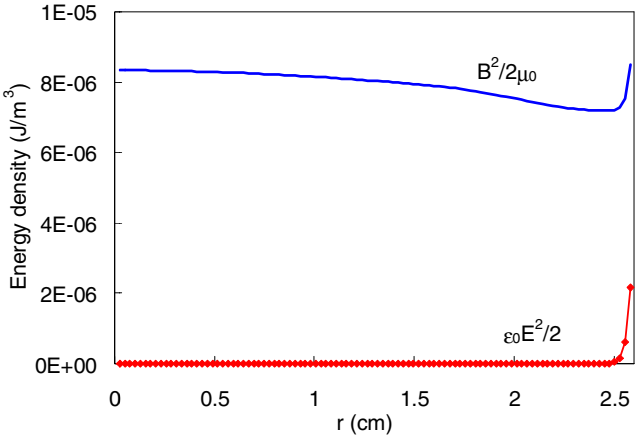

Figure 34. Energy densities of the RF B- and E-fields (not including B_0), plotted on the same scale, for the same uniform plasma as in figure 28.

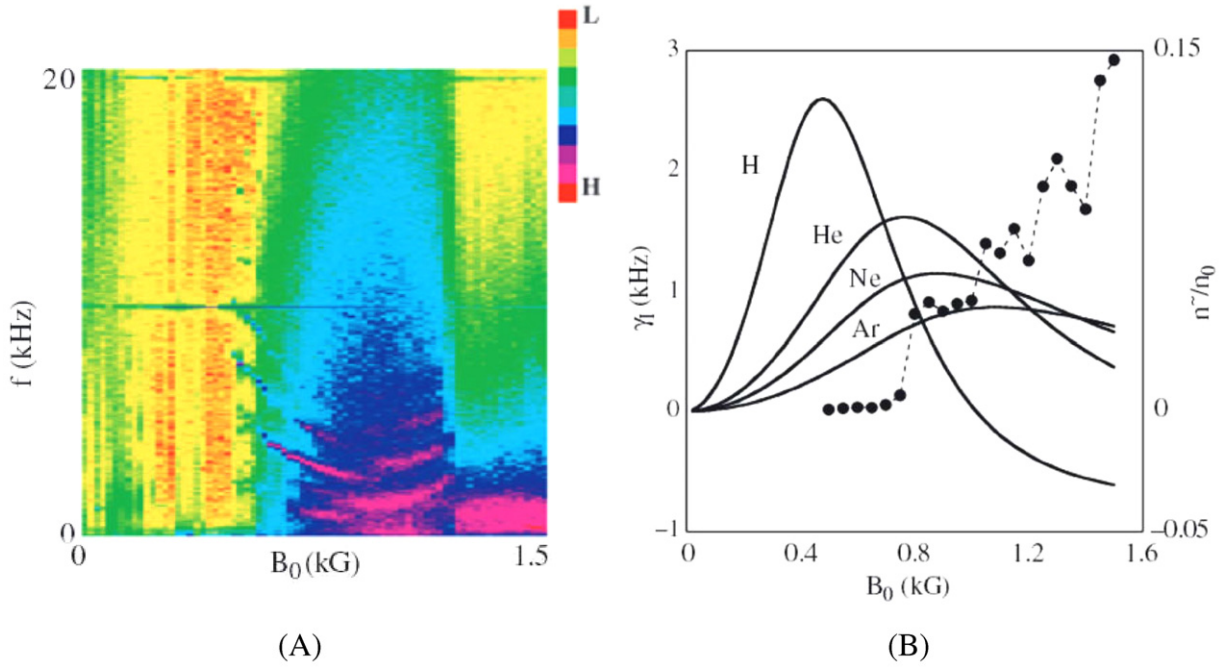

Figure 35. (*A*) Frequency spectrum versus B_0 in a neon helicon discharge and (*B*) measured growth rates γ_I in various gases (left-hand scale) and fractional instability amplitude (right-hand scale) [131].

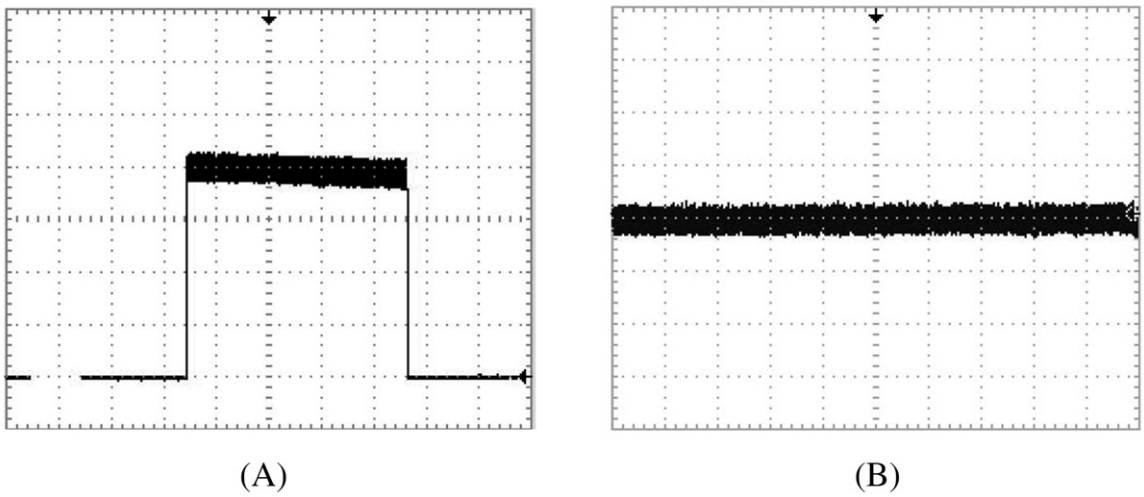

Figure 36. Oscilloscope traces of ion saturation current to a probe in a small helicon discharge. Sweep speeds are (*A*) 1 s/div and (*B*) 5 μs/div. The hash is a pure 27.12 MHz RF pickup [27]. Reproduced with permission from [27]. Copyright 2012, AIP Publishing LLC.

ignition may not occur; and then it is necessary to start the plasma at high pressure, say 30–40 mTorr, and then reduce to the operating pressure. Breakdown is more easily achieved at 27 MHz than at 13 MHz.

(9) Are helicons actually electrostatic, not electromagnetic, discharges?

The antenna mechanism of figure 7 shows that *electrostatic* fields are an essential element of this *inductive* discharge. In the absence of full scans of E-fields in a helicon discharge, we show HELIC calculations of these fields. Figure 33 shows radial plots of $|B|$ and $|E|$ for the H and TG modes separately. The H-mode has $|B|$ slightly peaked on axis and $|E|$ slightly peaked at the edge, while the TG mode has both strongly localized to the edge.

Although it would seem that the E-field, reaching 700 V at the edge, is dominant, it is the RF magnetic field that has most of the wave energy, as shown in figure 34. Thus, a helicon discharge is still quite different from a capacitive discharge, in spite of the fact that the RF energy enters mainly through electric fields at the edge.

12. Instabilities

Most helicon discharges are long enough to be subject to drift-wave type instabilities, which are driven by the necessary radial pressure gradient. Indeed, Light *et al* [131] have seen both discrete modes and turbulence in the 10 kHz regime, as

seen in figure 35(*a*). The nonlinear limit of the amplitudes increased with B_0 and their growth rates decreased with ion mass (figure 35(*b*)).

Tynan *et al* [132] have measured the anomalous transport in the sheared azimuthal $\boldsymbol{E} \times \boldsymbol{B}$ flow in a large helicon discharge (see section 10.4). As expected, the particle flux in the turbulent plasma is largest at the radius where $\mathrm{d}n/\mathrm{d}r$ is maximized.

Drift instabilities have long wavelength parallel to $\boldsymbol{B}_0$. They cannot arise in short plasmas. This has been confirmed by Chen [27] in a small helicon source 5 cm in diameter and 5 cm long. A trace of the ion saturation current to a probe is shown in figure 36. No low-frequency oscillations can be seen.

13. Versatility

During the past three decades of intense activity on helicon discharges, many types of machines have been built, large and small. Shinohara has built a large number of devices ranging from 2 to 74 cm in diameter [133–135]. Many experiments on dc electric fields in the plasma have been carried out by applying voltages to split endplates [136, 137]. Figure 37 gives an idea of what a large helicon discharge looks like [138]. The coils are 25 cm in inner diameter. Another large university installation is the HelCat machine of M. Gilmore [139] at the University of New Mexico, shown in figure 38.

An even larger helicon is being built for a spacecraft intended for travel to Mars, the VASIMR (Variable Specific Impulse Magnetoplasma Rocket) being built by Chang-Diaz [140]. A diagram is shown in figure 39. The plasma is further heated by ion cyclotron resonance heating. The possibility of parametric instabilities has been raised by Boswell *et al* [141]. The need for high-density plasmas for this purpose has inspired Squire, Winglee *et al* [142–144] to produce high-power, high-density helicons.

At the other extreme, a mini-thruster can be made with a 5 cm × 5 cm helicon tube and a permanent magnet. A picture of a prototype [27] of this proposed device is shown in figure 40. The simplicity of such single-loop antennas has also appealed to Shamrai [145] and to Carter and Khachan [146]. The large chamber in figure 40 has small permanent magnets covering the outside wall to help confine the plasma. This method had been used earlier by Charles [147].

Helicon sources have also been used to inject plasma into toroidal chambers. For instance, Loewenhardt *et al* used a helicon source to fill a toroidal heliac [149] fusion confinement device, and Sakawa *et al* [150] used helicons to fill a torus with hydrogen.

14. Applications

14.1. Plasma processing

The most obvious use of helicon sources was for etching and deposition in the manufacture of semiconductor circuits. The standard systems are capacitively coupled plasmas (CCPs) and inductively coupled plasmas (ICPs). CCPs are parallel plates with the silicon wafer mounted on the bottom one. RF on the top plate generates the plasma, and a bias on the bottom plate accelerates ions onto the wafer. CCPs are used mostly for deposition of silicon dioxide. ICPs use antennas on a dome above the wafer chuck to generate a plasma without a B-field. Helicon sources would generate higher plasma density and decrease the processing time, but they have not yet been accepted by the semiconductor industry.

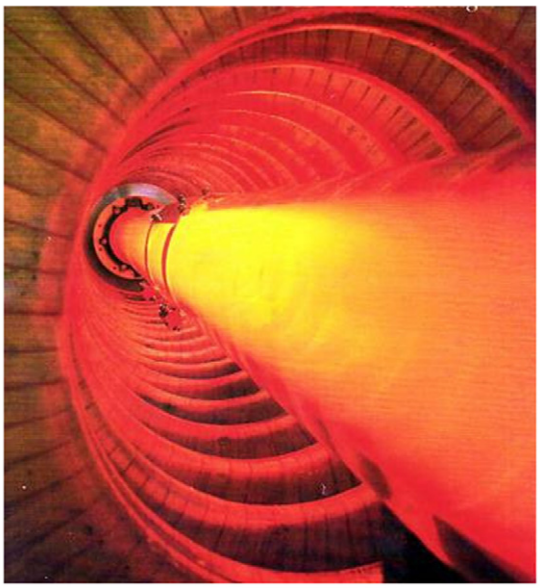

Figure 37. A large helicon source at the University of Wisconsin [138].

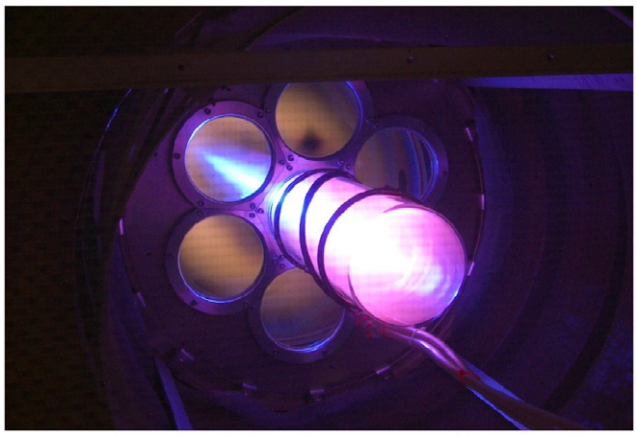

Figure 38. The HelCat helicon machine [139]. Picture by the author.

The first helicon built for commercial use was that of Benjamin *et al* [151] in 1991. This source by Lucas Labs was compared with ECR sources in three papers by Tepermeister *et al* [152–154]. They found that the Lucas source was not better than an ECR source in etch rate but gave somewhat better uniformity.

A few years later, a company called PMT, Inc. was formed in Chatsworth, CA, by Conn and Campbell, with advice from Shoji and the author, to manufacture the MØRI ($m = 0$ reactive ion etcher) plasma source [155] shown in figure 41. This used a two-ring antenna with opposite currents. The B-field was provided by two coaxial coils, with the outer one

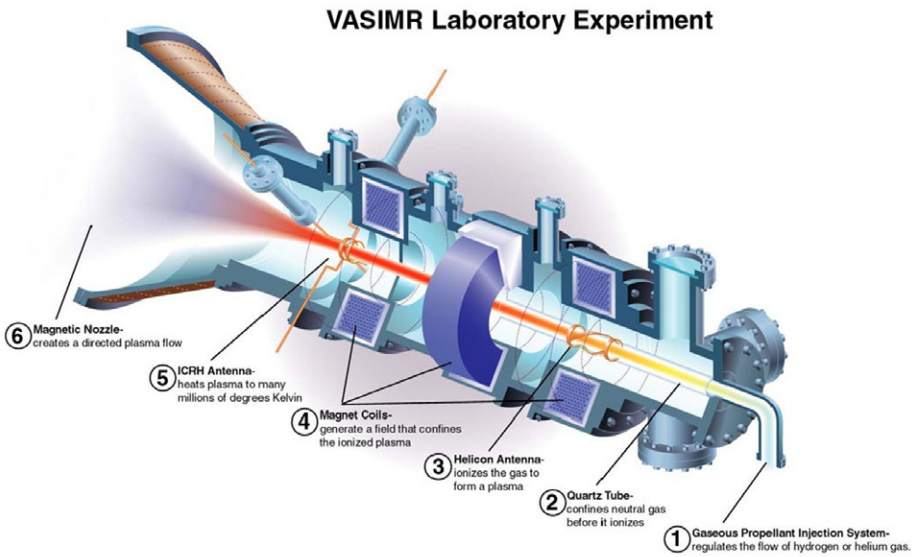

Figure 39. Diagram of the VASIMR [148].

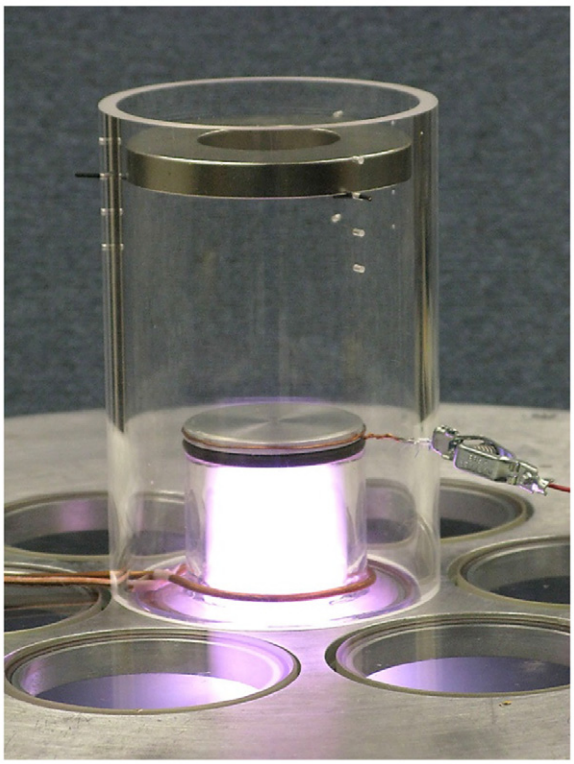

Figure 40. Photo of a 5 cm diameter helicon source using the remote field of a permanent magnet [27]. Reproduced with permission from [27]. Copyright 2012, AIP Publishing LLC.

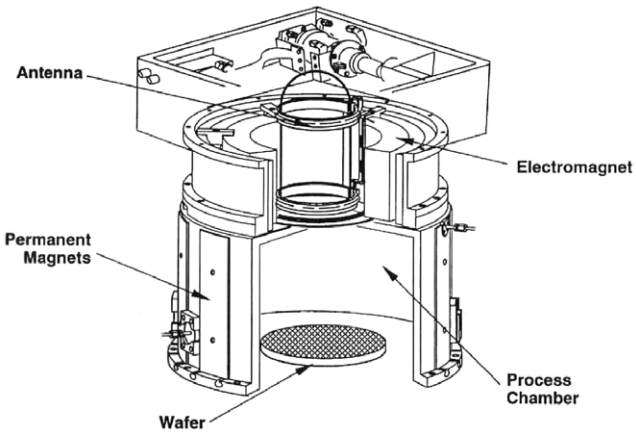

Figure 41. The MØRI helicon source [155]. The matching circuit is sketched above it. Reproduced with permission from [155]. Copyright [1997], American Vacuum Society.

carrying a current in the opposite direction so as to flare out the field, preventing it from reaching the substrate. This source passed 'marathon' tests for endurance and was even made into a cluster tool for cleaning, etching, and deposition steps in semiconductor production. The company failed due to a poor business decision.

At the time, the state of the art was in 300 mm (12 inch) diameter silicon substrates. To cover such an area uniformly with dense plasma, experiments were done with arrays of helicon sources. To produce uniform coverage of the substrate, an array of tubes such as the one shown in figure 42(*a*) was envisioned. The seven tubes would actually be arrayed as in figure 43. However, this arrangement would suffer losses to the top flange, as shown in figure 42(*b*). To solve this, the B-field must be generated by a large electromagnet covering all the tubes, as in figure 44. The small tubes shown there are prototypes of the tube shown in figure 40. Density profiles of this array source, seen in figure 45, showed good uniformity over a surface 40 cm in diameter [156]. The 2D plot of the density in figure 46 shows no trace of the sixfold symmetry of the sources. To eject plasma toward a substrate requires allowing the plasma to leave the magnetic field lines. A test of ejection was carried out by Jiang in Chen *et al* [157]. Smooth, peaked density profiles were measured downstream, but the densities were low because the field lines that reach the substrate originate from only a small central column of the discharge (figure 42(*b*)). The rest is lost to the walls.

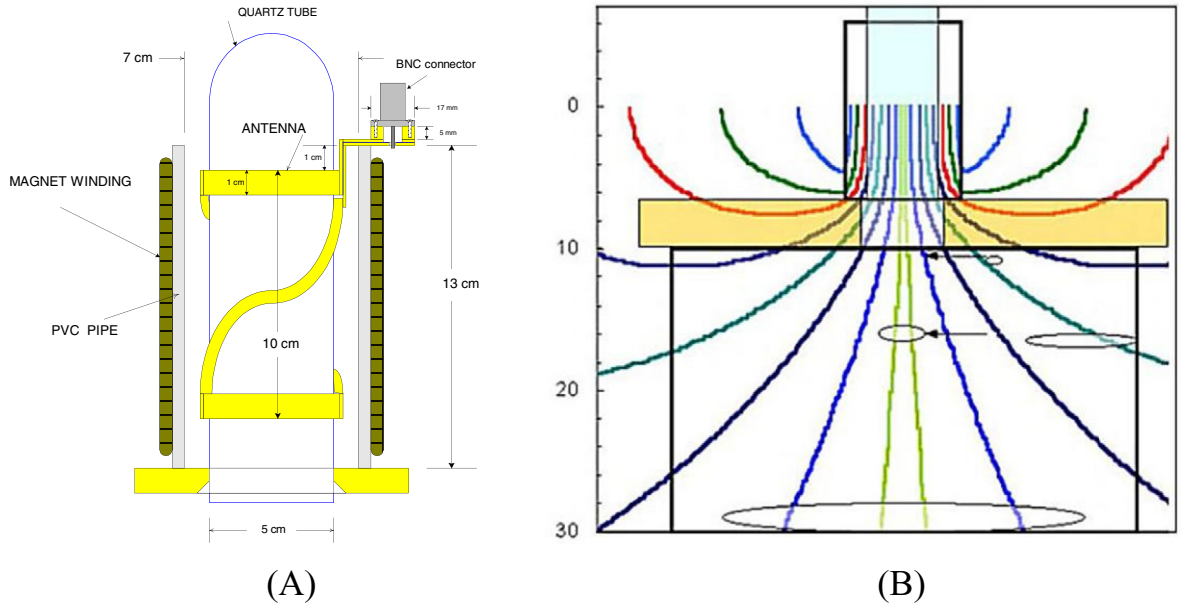

Figure 42. (*a*) Diagram of a small helicon source with its own magnet coil and helical antenna. (*b*) Field lines from this source and the sizes of electron Larmor orbits at various downstream locations [157]. Reproduced with permission from [157]. Copyright [2000], American Vacuum Society.

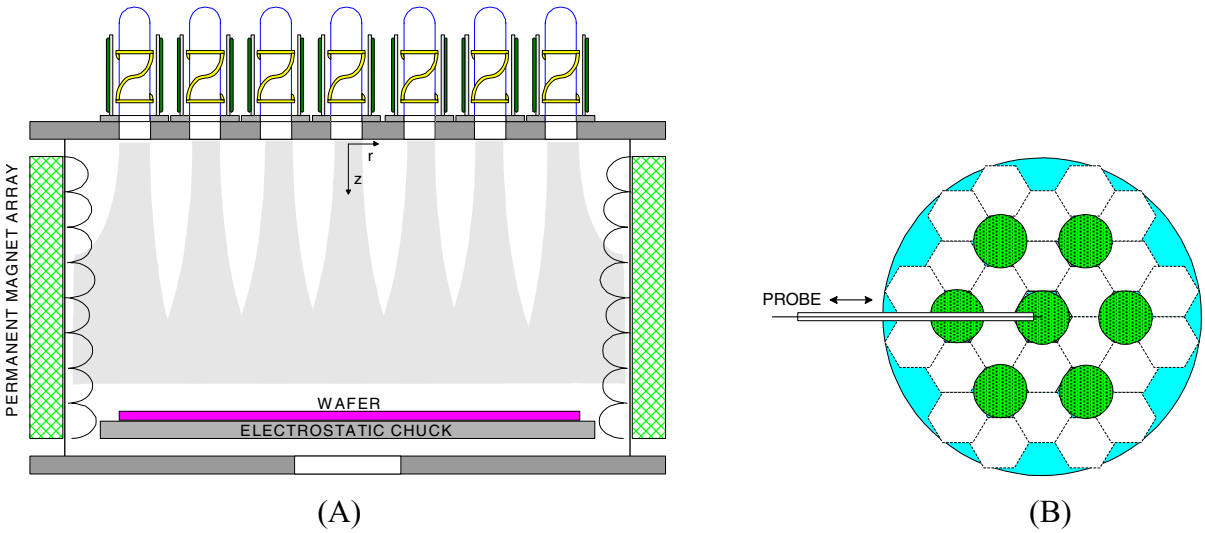

Figure 43. (*a*) Proposed array of seven helicon sources. Radial confinement is improved by covering the walls with small permanent magnets. (*b*) Actual circular arrangement of the seven sources.

The necessity for such a large electromagnet made the device impractical for large-scale manufacturing, and it was not adopted by the semiconductor industry. This constraint has been largely alleviated by the use of permanent magnets. PM helicons will be described in a later section.

14.2. Spacecraft propulsion

Modern satellites boosted into space use ejection of ions, usually xenon, to achieve the proper orbital velocity. These thrusters are of two types. Gridded ion thrusters create a plasma by accelerating electrons from a thermionic emitter toward an anode. A grid then holds back the electrons while another grid accelerates the ions to high velocity in the exhaust. Electrons are emitted from an external source to neutralize the charges of the ejected ions, keeping the spacecraft from charging up. Hall thrusters also accelerate the ions by applying an electric field, but the electrons are held back instead by a dc magnetic field. An external electron source is still needed to neutralize the ion beam. Helicon thrusters eject a neutral plasma, both ions and electrons, and no neutralizer is necessary. Straightforward application of helicons to Hall thrusters would require helicon waves in an annular geometry. This configuration has been studied by Yano and Walker [158].

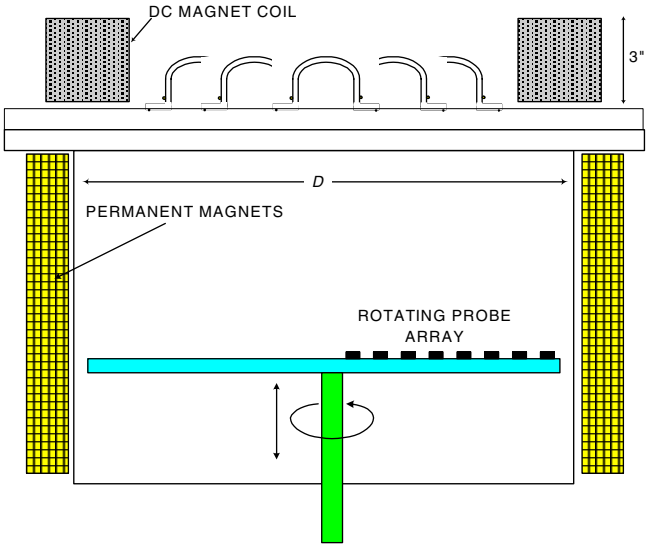

Figure 44. An array of seven small tubes with a large magnet providing the B-field.

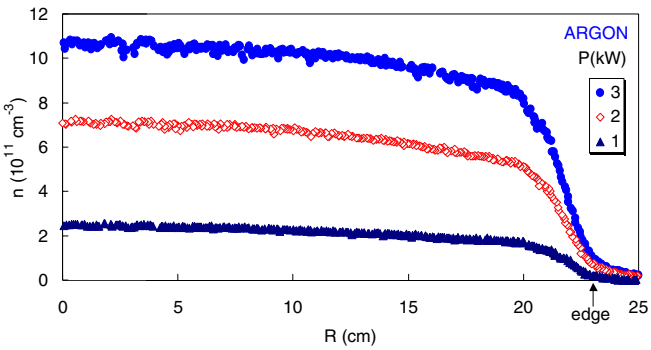

Figure 45. Radial density profiles in the array source of figure 44 [156]. Similar uniformity also occurred in chlorine plasmas.

Thrusters are characterized by their specific impulse, measured in seconds, which is their exhaust velocity compared with the velocity of a rock dropped from rest for that many seconds under the Earth's surface gravity [159]. A helicon thruster has the advantage that ions are accelerated by a sudden drop in space potential, called a 'double layer', in the plasma ejected by the source. The double layer is simply a sheath in space. It is well known that if monoenergetic ions are accelerated to the 'Bohm velocity', which is just the acoustic velocity $c_s = (KT_e/M_i)^{1/2}$, the ion density in a falling potential will be larger than the Maxwellian electron density, and this will cause the potential to fall further, creating the sheath on a wall [160]. This can also occur in free space, where electrons will rush in to cancel the ion charge, creating a double layer (figure 47). C. Charles has written a review of double layers [161].

There is a large literature on this complicated phenomenon. To give the reader an idea of why it occurs, we give a simplified calculation [162] of the location of the double layer when the B-field lines are diverging, as in figure 48. For

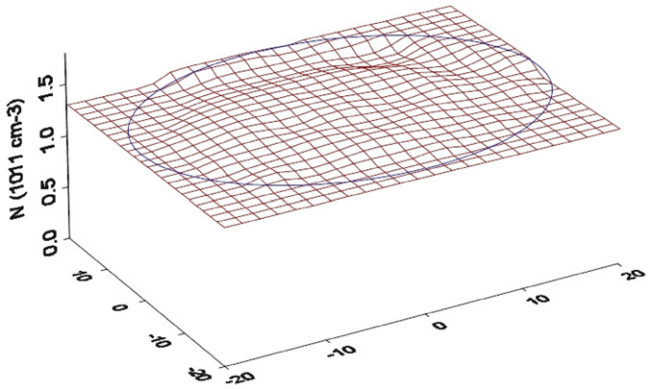

Figure 46. 2D plot of density from a seven-tube source ([156]; figure omitted from final publication).

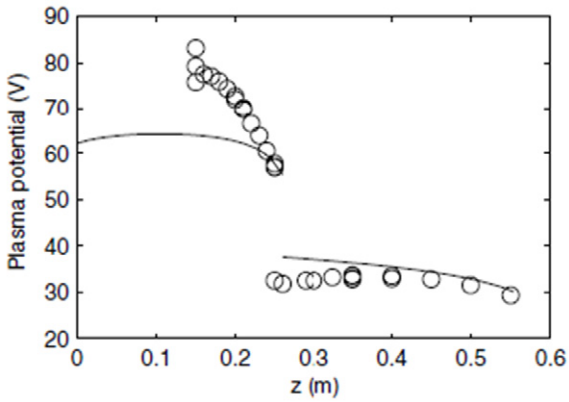

Figure 47. Observation of the potential jump associated with a double layer in free space [161].

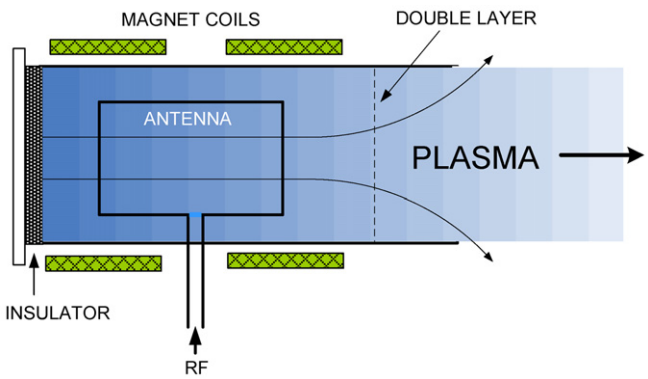

Figure 48. Location of the double layer downstream of a helicon discharge.

Maxwellian electrons, the plasma density is given by

$$n_e = n_0 e^{-\eta}, \quad \text{where} \quad \eta = -eV/KT_e. \tag{11}$$

The Bohm energy is

$$v_{is} = c_s = (KT_e/M)^{(1/2)} \quad \therefore W_{is} = 1/2Mv_{is}^2 = 1/2KT_e. \tag{12}$$

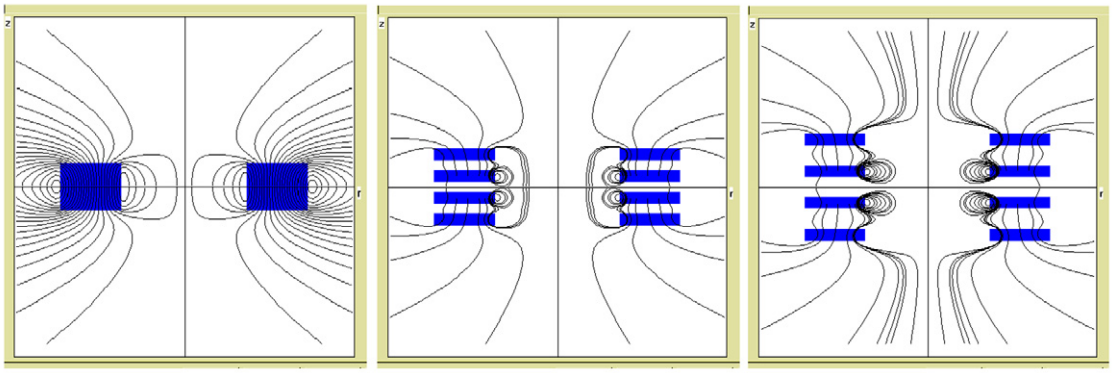

Figure 49. Examples of field patterns from different magnet arrays.

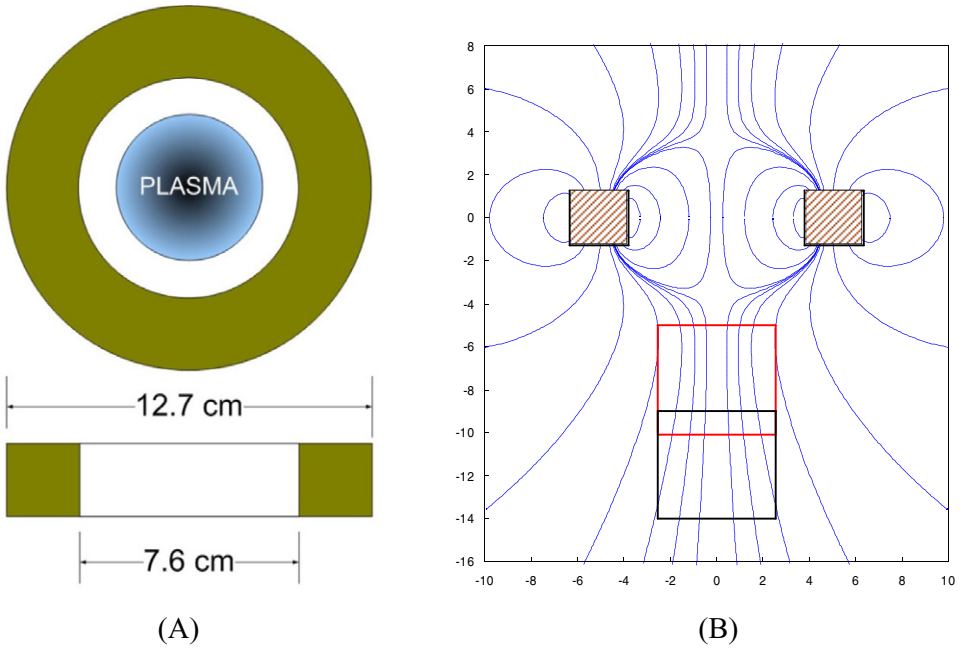

Figure 50. (*a*) The designed magnet. (*b*) Field lines of the magnet. The squares show two possible positions of the discharge tube in the remote field.

To gain this energy, ions must have been accelerated by a sheath potential $\eta_s = 1/2$

$$\therefore \quad \eta_s = 1/2, \quad n_s/n_0 = e^{-1/2}, \quad B/B_0 = n/n_0 = (r_0/r)^2, \quad r/r_0 = e^{1/4} = 1.28. \tag{13}$$

A single layer (an ion sheath) forms where r has increased by 28%. In the absence of a wall, electrons will be attracted to the positive charge and shield it, forming a double sheath.

On the subject of thrusters, there are several papers on the shape of the plume, or magnetic nozzle, of plasma emitted [163–166]. These details are outside the scope of this paper. Upon satellite re-entry, a plasma of density $\approx 10^{17}\,\mathrm{m}^{-3}$ is formed by the nosecone striking the atmosphere. Lemmer *et al* [167] have simulated these plasma conditions with a helicon source.

15. Permanent-magnet helicons

The dc magnetic field that helicons require has impeded their acceptance in industry. It is possible, however, to use permanent magnets to produce long, quasi-uniform B-fields. This may be an important development in helicon design for such practical applications as semiconductor etching and spacecraft propulsion. Takahashi [168] has used straight PMs, but most work has been done by Chen [27] with annular magnets. That system will serve as an example for what can be done with PMs. When polarized vertically, the B-field of ring magnets has a stagnation point not far below the magnet, and the field below this point, though much weaker than that inside the hole, is fairly uniform and extends to infinity (see figure 50(*b*) later). Neodymium (NeFeB) magnets have fields above 1 T inside, and even in the remote field below the stagnation point a field of 30–200 G is available for helicon experiments.

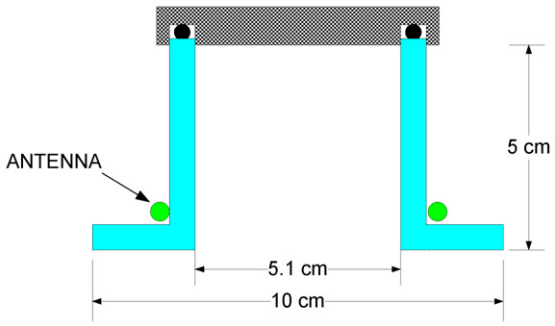

Figure 51. Final design of the discharge tube.

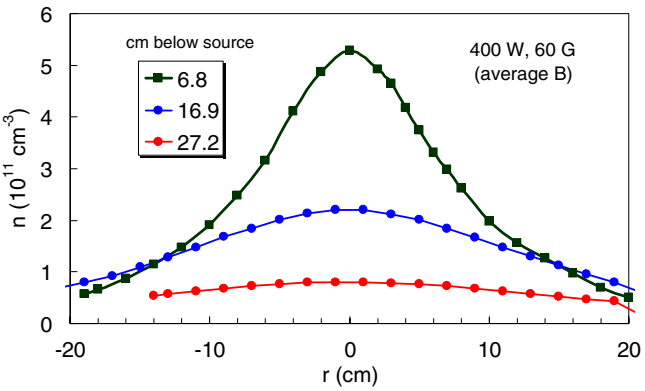

Figure 52. Radial density profiles downstream from the source of figure 50. Reproduced with permission from [27]. Copyright 2012, AIP Publishing LLC.

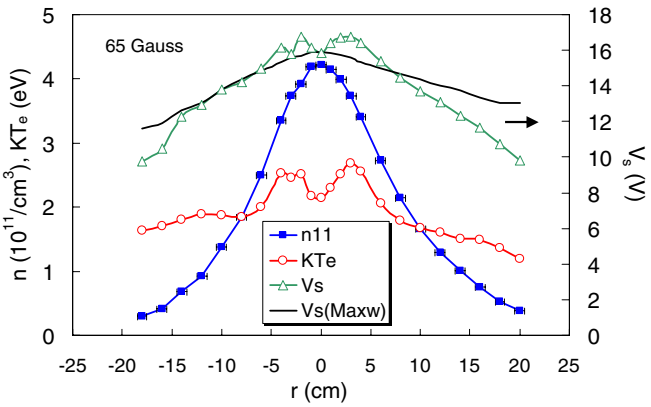

Figure 53. Radial profiles in port 1 [27] at 400 W. Density and KT_e are both shown on the left-hand scale, while space potential V_s is shown on the right-hand scale. Reproduced with permission from [27]. Copyright 2012, AIP Publishing LLC.

15.1. B-field design

The field patterns of various ring magnet designs with different numbers of rings and different spacings between them were computed, as shown in figure 49, but there was no advantage over a single ring. The final design suitable for coverage of a 5 cm × 5 cm tube is shown in figure 50(*a*).

15.2. Tube design

The diameter and length of the discharge tube were determined by computing the plasma resistance R with the HELIC code.

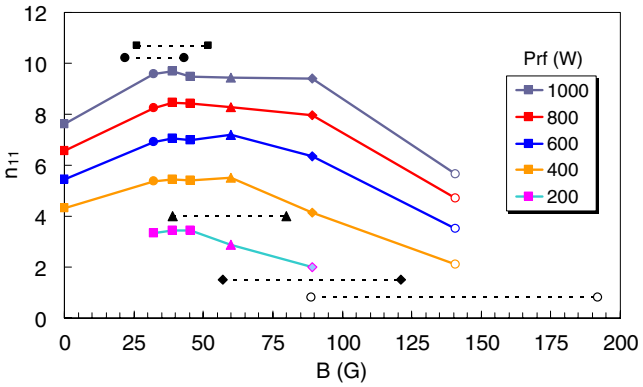

Figure 54. Peak density in port 2, 16.9 cm below the tube, versus B_0 and P_{rf} [27]. The dashed lines indicate the range of B-field within the 5 cm height of the tube. Each dashed line corresponds to the curve with the same symbol above or below the center of the line. Reproduced with permission from [27]. Copyright 2012, AIP Publishing LLC.

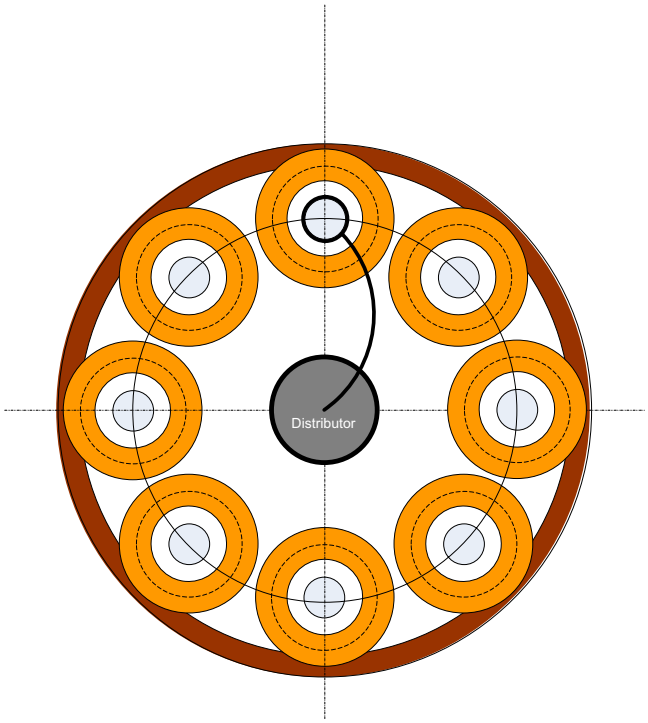

Figure 55. Design for an eight-tube array source. The power from a matching circuit is fed in parallel to the tubes through a distributor, one arm of which is shown.

The results were organized in matrices showing the variations with tube radius and length, RF frequency, gas pressure, and top plate material. The final design is shown in figure 51.

.

15.3. Performance

The source of figure 50(*b*) has been used to inject plasma to fill a large experimental chamber, and extensive measurements of the plasma downstream have been made [27]. Figure 52 shows density profiles there, following normal collisional diffusion.

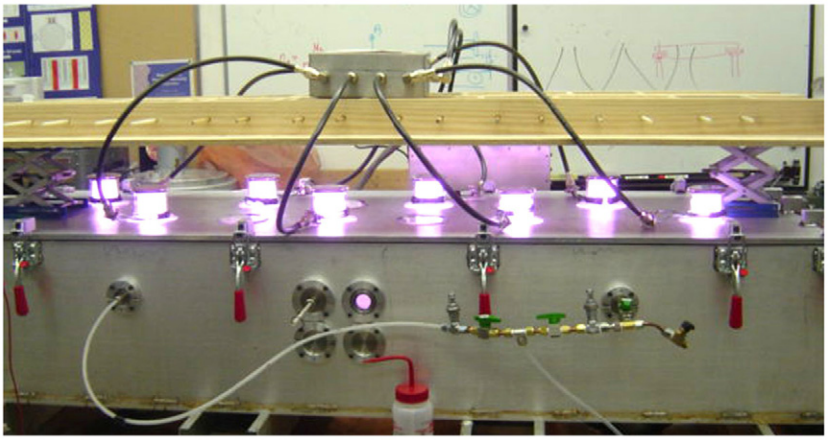

Figure 56. An eight-tube array of small helicon sources [170, 171]

Figure 53 shows details in port 1, just 6.8 cm below the source. The $n(r)$ curve is the same as that in (figure 52). The KT_e curve shows two peaks due to the TG mode. The plasma (space) potential V_s is shown by dots as measured from the 'knee' of Langmuir probe traces and agrees reasonably well with V_s calculated from the Boltzmann equation, knowing n and T_e (line).

Figure 54 shows peak density 16.9 cm below the source versus B-field and RF power. The density does not rise monotonically with B_0 because of insufficient power to reach the peaks shown in figure 14. The density actually decreases at high B_0 because the discharge falls out of resonance. This graph shows that B-fields no higher than about 30–60 G are sufficient for applications requiring $n \leqslant 10^{12}\,\mathrm{cm}^{-3}$. In that case, the large magnet of figure 50 is not necessary and can be replaced by an off-the-shelf Nd magnet such as that in figure 40.

15.4. PM arrays

Plasma processing requires uniform coverage of large substrates with plasma densities of order 10^{10}–$10^{11}\,\mathrm{cm}^{-3}$. The semiconductor industry is advancing to 400 mm diameter silicon. This presents an opportunity for helicons to penetrate the market. A uniform plasma can be produced by a circular array of small helicon sources such as those shown in figures 50 and 51. A diagram of such an array is shown in figure 55. A theory by Chen and Curreli [169] shows that sources at the edge, with no center source, can produce a plasma uniform to the center. In roll-to-roll processing, a wide plasma source can be used to treat a substrate moving underneath. Such a helicon source is shown in figure 56. The tubes are in two rows and can be arranged either opposite one another or staggered. The RF is fed via Teflon-insulated cables of equal length to each tube. All connections are soldered, since coaxial connectors will arc over with the voltages applied. When 400 W or more is applied to each tube in parallel, all will light up equally. The magnet rack and distribution box are shown in figure 57. Finally, figure 58 shows the helicon array powered from a rectangular 50 Ω transmission line in which the center conductor is a copper tube carrying both the RF and the cooling water. The water is connected to the tube in pairs, so that it enters and leaves the system at ground potential on the top and bottom flanges of the transmission line. The plasma uniformity at the bottom of the chamber is ±3%.

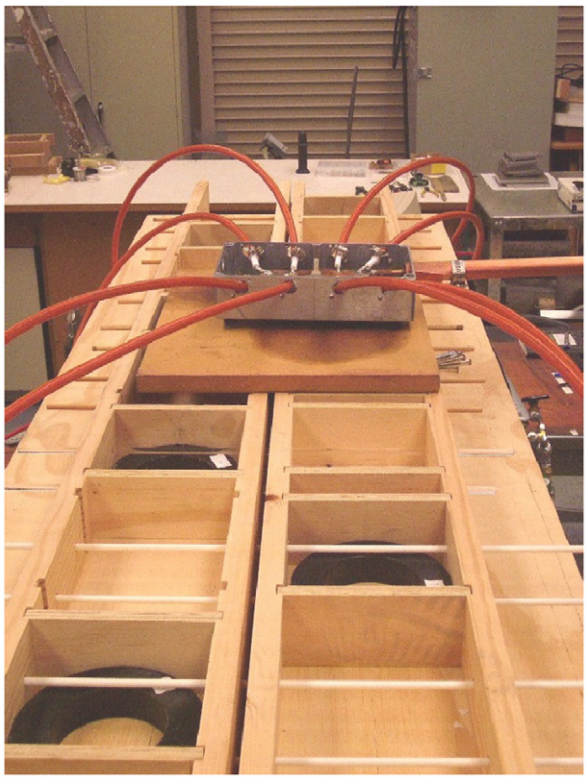

Figure 57. The distribution box and the magnet rack with movable partitions.

Acknowledgments

My quarter-century of work on helicons would not have been possible without the friendship of and collaboration with three theorists: John Dawson (d. 2001), Don Arnush (d. 2003) and Konstantin (Kostia) Shamrai (d. 2013). John contributed the

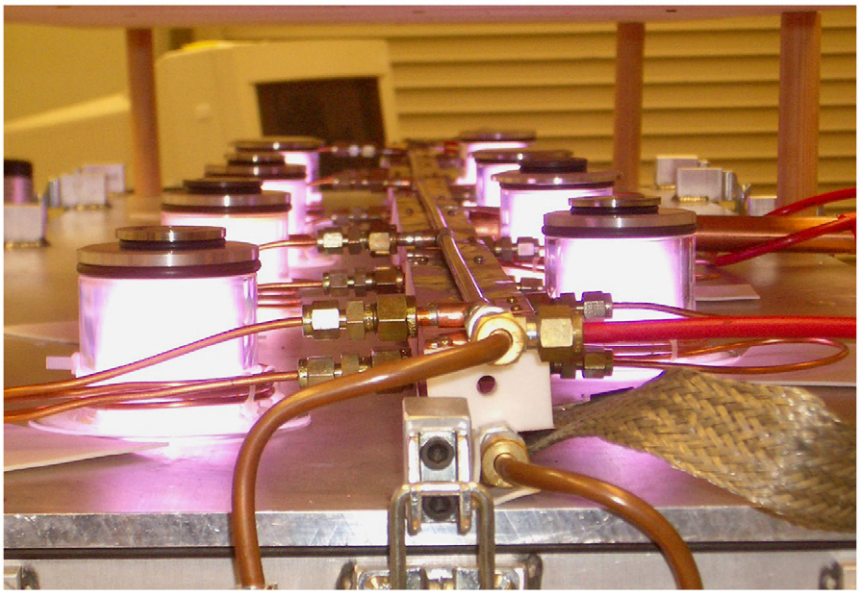

Figure 58. An eight-tube PM helicon array powered from a rectangular 50 Ω transmission line.

Nagoya type III antenna mechanism and taught me how to think physically without equations.

References

[1] Lehane J A and Thonemann P C 1965 *Proc. Phys. Soc.* **85** 301
[2] Aigrain P 1960 Les 'helicons' dans les semiconducteurs *Proc. Intl. Conf. on Semiconductor Physics (Prague, Czech Republic, 1960)* (London: Butterworths) p 224
[3] Woods L 1962 *J. Fluid Mech.* **13** 570
[4] Woods L 1964 *J. Fluid Mech.* **18** 401
[5] Legendy C R 1964 *Phys. Rev.* A **135** 1713
[6] Legendy C R 1965 *J. Math. Phys.* **6** 153
[7] Klozenberg J P, McNamara B and Thonemann P C 1965 *J. Fluid Mech.* **21** 545
[8] Bleven H A and Christiansen P J 1966 *Aust. J. Phys.* **19** 501
[9] Bleven H A and Christiansen P J 1968 *Plasma Phys.* **10** 799
[10] Bleven H A, Christiansen P J and Davies B 1968 *Phys. Rev. Lett.* A **8** 230
[11] Ferrari R L and Klozenberg J P 1968 *J. Plasma Phys.* **2** 283
[12] Davies B J and Christiansen P J 1969 *Plasma Phys.* **11** 987
[13] Shoucri M M 1969 *Plasma Phys.* **11** 1017
[14] Boswell R W 1970 *Phys. Lett.* A **33** 457
[15] Shoji T, Sakawa Y, Nakazawa S, Kadota K and Sato T 1993 *Plasma Sources Sci. Technol.* **2** 5
[16] Tynan G R *et al* 1997 *J. Vac. Sci. Technol.* A **15** 2885
[17] Chapman B, Benjamin N, van Os C F A, Boswell R W and Perry A J 1991 Plasma dry processing in the helicon reactor *12th Symp. on Dry Process (Denki-Gakkai, Tokyo, Japan, 1991)*
[18] ISI Web of Knowledge
[19] Boswell R W 1972 *Aust. J. Phys.* **25** 403
[20] Boswell R W 1984 *Plasma Phys. Control. Fusion* **26** 1147
[21] Chen F F 1991 *Plasma Phys. Control. Fusion* **33** 339
[22] Chen F F 1995 Helicon plasma sources *High Density Plasma Sources* ed O A Popov (Park Ridge, NJ: Noyes) ch 1
[23] Arnush D 2000 *Phys. Plasmas* **7** 3042
[24] www.seas.ucla.edu/ltptl/presentations.htm
[25] Charles C 2007 *Plasma Sources Sci. Technol.* **16** R1
[26] Takahashi K, Oguni K, Yamada H and Fujiwara T 2008 *Phys. Plasmas* **15** 084501
[27] Chen F F 2012 *Phys. Plasmas* **19** 093509
[28] Li W, Ruan Y, Luther-Davies B, Rode A and Boswell R 2005 *J. Vac. Sci. Technol.* A **23** 1626
[29] Squire J P, Chang-Diaz F R, Glover T W, Jacobson V T, McCaskill G E, Winter D S, Baity F W, Carter M D and Goulding R H 2006 *Thin Solid Films* **506** 579
[30] Chen F F 1997 *Phys. Plasmas* **3** 1783
[31] Trivelpiece A W and Gould R W 1959 *J. Appl. Phys.* **30** 1784
[32] Chen F F 1984 *Introduction to Plasma Physics and Controlled Fusion* vol 1 *Plasma Physics* 2nd edn (New York: Plenum) p 106
[33] Boswell R W 1984 *J. Plasma Phys.* **31** 197
[34] Shamrai K P and Taranov V B 1996 *Plasma Sources Sci. Technol.* **5** 474
[35] Borg G G and Boswell R W 1998 *Phys. Plasmas* **5** 564
[36] Chen F F and Arnush D 1997 *Phys. Plasmas* **4** 3411
[37] Blackwell D D, Madziwa T G, Arnush D and Chen F F 2002 *Phys. Rev. Lett.* **88** 145002
[38] Watari T *et al* 1978 *Phys. Fluids* **21** 2076
[39] Chen F F 1991 Double helix: the Dawson separation process *From Fusion to Light Surfing* ed T Katsouleas (New York: Addison-Wesley) ch 14
[40] Chen F F 1981 Radiofrequency field enhancement near ion gyroresonance *TRW Report Task* II-3552 www.ee.ucla.edu/~ffchen/Archive/Chen095.pdf.
[41] Miljak D G and Chen F F 1998 *Plasma Sources Sci. Technol.* **7** 61
[42] Chen F F 1995 Helicon plasma sources *High Density Plasma Sources* ed O A Popov (Park Ridge, NJ: Noyes) p 60
[43] Loewenhardt P K, Blackwell B D, Boswell R W, Conway G D and Hamberger S M 1991 *Phys. Rev. Lett.* **67** 2792
[44] Zhu P and Boswell R W 1991 *Phys. Fluids* B **3** 869
[45] Ellingboe A R, Boswell R W, Booth J P and Sadeghi N 1995 *Phys. Plasmas* **2** 1807
[46] Molvik A W, Ellingboe A R and Rognlien T D 1997 *Phys. Rev. Lett.* **79** 233
[47] Chen F F and Blackwell D D 1999 *Phys. Rev. Lett.* **82** 2677
[48] Cho S 1996 *Phys. Plasmas* **3** 4268
[49] Kamenski I V and Borg G G 1998 *Comput. Phys. Commun.* **113** 10
[50] Curreli D and Chen F F 2011 *Phys. Plasmas* **18** 113501
[51] Guo X M, Scharer J, Mouzouris Y and Louis L 1999 *Phys. Plasmas* **6** 3400
[52] www.seas.ucla.edu/ltptl/presentations.htm (HELIC 10zip.exe)

[53] Stix T H 1992 *Waves in Plasmas* (New York: Springer)
[54] Arnush D and Chen F F 1998 *Phys. Plasmas* **5** 1239
[55] Shamrai K P 1998 *Plasma Sources Sci. Technol.* **7** 499
[56] Cho S 1996 *Phys. Lett.* A **216** 137
[57] Cho S 1996 *Phys. Plasmas* **3** 4268
[58] Cho S and Kwak J G 1997 *Phys. Plasmas* **4** 4167
[59] Cho S and Lieberman M A 2003 *Phys. Plasmas* **10** 882
[60] Chen F F 1992 *J. Vac. Sci. Technol.* A **10** 1389
[61] Chen F F 2003 *Phys. Plasmas* **10** 2586
[62] Degeling A W, Jung C O, Boswell R W and Ellingboe A R 1996 *Phys. Plasmas* **3** 2788
[63] Sato G, Oohara W and Hatakeyama R 2007 *Plasma Sources Sci. Technol.* **16** 734
[64] Cho S 2006 *Phys. Plasmas* **13** 033504
[65] Zhu P and Boswell R W 1990 *J. Appl. Phys.* **68** 1981
[66] Degeling A W and Boswell R W 1997 *Phys. Plasmas* **4** 2748
[67] Chi K, Sheridan T E and Boswell R W 1999 *Plasma Sources Sci. Technol.* **8** 421
[68] Ellingboe A R and Boswell R W 1996 *Phys. Plasmas* **3** 2797
[69] Chen F F and Torreblanca H 2007 *Plasma Sources Sci. Technol.* **16** 593
[70] Chevalier G and Chen F F 1993 *J. Vac. Sci. Technol.* A **11** 1165
[71] Blackwell D D and Chen F F 1997 *Plasma Sources Sci. Technol.* **6** 569
[72] Light M and Chen F F 1995 *Phys. Plasmas* **2** 1084
[73] Light M, Sudit I D, Chen F F and Arnush D 1995 *Phys. Plasmas* **2** 4094
[74] Shinohara S and Tanikawa T 2004 *Rev. Sci. Instrum.* **75** 1941
[75] Shinohara S and Tanikawa T 2005 *Phys. Plasmas* **12** 044502
[76] Motomura T, Shinohara S, Tanikawa T and Shamrai K P 2012 *Phys. Plasmas* **19** 043504
[77] Shinohara S and Soejima T 1998 *Plasma Phys. Control. Fusion* **40** 2081
[78] Shinohara S, Kaneda N and Kawai Y 1998 *Thin Solid Films* **316** 139
[79] Shinohara S, Takechi S, Kaneda N and Kawai Y 1997 *Plasma Phys. Control. Fusion* **39** 1479
[80] Shinohara S and Shamrai K P 2000 *Plasma Phys. Control. Fusion* **42** 865
[81] Kuwahara D, Mishio A, Nakagawa T and Shinohara S 2013 *Rev. Sci. Instrum.* **84** 103502
[82] Shinohara S, Tsuji H, Yoshinaka T and Kawai Y 1999 *Surf. Coat. Technol.* **112** 20
[83] Shinohara S, Matsuoka N and Yoshinaka T 1999 *Japan. J. Appl. Phys.* **38** 4321
[84] Shinohara S, Matsuoka N and Matsuyama S 2001 *Phys. Plasmas* **8** 1154
[85] Scime E E, Keesee A M and Boswell R W 2008 *Phys. Plasmas* **15** 058301 http://ulysses.phys.wvu.edu/ESCIME/miniconference/2007postersession.html
[86] Balkey M M, Boivin R, Kline J L and Scime E E 2001 *Plasma Sources Sci. Technol.* **10** 284
[87] Kline J L, Scime E E, Boivin R F, Keesee A M, Sun X and Mikhailenko 2002 *Phys. Rev. Lett.* **88** 195002
[88] Kline J L and Scime E E 2003 *Phys. Plasmas* **10** 135
[89] Krämer M, Aliev Yu M, Altukhov A B, Gurchenko A D, Gusakov E Z and Niemi K 2007 *Plasma Phys. Control. Fusion* **49** A167
[90] Lorenz B, Krämer M, Selenin V L and Aliev Yu M 2005 *Plasma Sources Sci. Technol.* **14** 623
[91] Fischer B, Krämer M and Enk Th 1994 *Plasma Phys. Control. Fusion* **36** 2003
[92] Sakawa Y, Takino T and Shoji T 1998 *Appl. Phys. Lett.* **73** 1643
[93] Sakawa Y, Koshikawa N and Shoji T 1997 *Plasma Sources Sci. Technol.* **6** 96
[94] Sakawa Y, Takino T and Shoji T 1999 *Phys. Plasmas* **6** 4759
[95] Mori Y, Nakashima H, Baity F W, Goulding R H, Carter M D and Sparks D O 2004 *Plasma Sources Sci. Technol.* **13** 424
[96] Yun S-M, Kim J-H and Chang H-Y 1997 *J. Vac. Sci. Technol.* A **15** 673
[97] Kim J H, Yun S M and Chang H Y 1996 *IEEE Trans. Plasma Sci.* **24** 1364
[98] Yun S M, Kim J H and Chang H Y 1998 *IEEE Trans. Plasma Sci.* **26** 159
[99] Yun S M, Cho S, Tynan G and Chang H Y 2001 *Phys. Plasmas* **8** 358
[100] Kim J H and Chang H Y 1996 *Phys. Plasmas* **3** 1462
[101] Eom G S, Bae I D, Cho G, Hwang Y S and Choe W 2001 *Plasma Sources Sci. Technol.* **10** 417
[102] Eom G S and Choe W 2002 *J. Vac. Sci. Technol.* A **20** 2079
[103] Eom G S, Kim J and Choe W 2006 *Phys. Plasmas* **13** 73505
[104] Loewenhardt P K, Blackwell B D and Hamberger S M 1995 *Plasma Phys. Control. Fusion* **37** 229
[105] Zhang B C, Borg G G and Blackwell B D 1995 *Plasma Phys.* **2** 803
[106] Chang L, Hole M J, Caneses J F, Chen G, Blackwell B D and Corr C S 2012 *Phys. Plasmas* **19** 083511
[107] Franck C M, Grulke O, Stark A, Klinger T, Scime E E and Bonhomme G 2005 *Plasma Sources Sci. Technol.* **14** 226
[108] Corr C S, Plihon N, Chabert P, Sutherland O and Boswell R W 2004 *Phys. Plasmas* **11** 4596
[109] Corr C S, Plihon N and Chabert P 2006 *J. Appl. Phys.* **99** 103302
[110] Petri R, Sadeghi N and Henry D 1996 *J. Vac. Sci. Technol.* A **13** 2930
[111] Sahu B B and Dangi A 2011 *Dronacharya Res. J.* **3** 89
[112] Sahu B B 2012 *Dronacharya Res. J.* **4** 17
[113] Ganguli A, Sahu B B and Tarey R D 2007 *Phys. Plasmas* **14** 113503
[114] Ganguli A, Sahu B B and Tarey R D 2013 *Phys. Plasmas* **20** 013510
[115] Paul M K and Bora D 2007 *Phys. Plasmas* **14** 082507
[116] Anitha V P, Sharma D, Banerjee S P and Mattoo S K 2012 *Phys. Plasmas* **19** 082118
[117] Tarey R D, Sahu B B and Ganguli A 2012 *Phys. Plasmas* **19** 073520
[118] Barada K K, Chattopadhyay P K, Ghosh J, Kumar S and Saxena Y C 2013 *Phys. Plasmas* **20** 012123
[119] Gilland J, Breun R and Hershkowitz N 1998 *Plasma Sources Sci. Technol.* **7** 418
[120] Chen R T S and Hershkowitz N 1998 *Phys. Rev. Lett.* **80** 4677
[121] Guo X M, Scharer J, Mouzouris Y and Louis L 1999 *Phys. Plasmas* **6** 3400
[122] Mouzouris Y and Scharer J E 1999 *IEEE Trans. Plasma Sci.* **27** 66
[123] Reilly M P and Miley G H 2010 *Plasma Sources Sci. Technol.* **19** 045006
[124] Tynan G R, Burin M J, Holland C, Antar G and Crocker N 2004 *Phys. Plasmas* **11** 5195
[125] Diamond P H and Kim Y-B 1991 *Phys. Fluids* B **3** 1626
[126] Holland C, Yu J H, James A, Nishijima D, Shimada M, Tahori N and Tynan G R 2006 *Phys. Rev. Lett.* **96** 195002
[127] Thakur S C, McCarren D, Lee T, Fedorczak N, Manz P, Scime E E, Tynan G R and Xu M 2012 *Phys. Plasmas* **19** 082102
[128] Breizman B N and Arefiev A V 2000 *Phys. Rev. Lett.* **84** 3863
[129] Breizman B N and Arefiev A V 2001 *Phys. Plasmas* **9** 1015
[130] Porte L, Yun S M, Chen F F and Arnush D 2003 *Plasma Sources Sci. Technol.* **12** 287
[131] Light M, Chen F F and Colestock P L 2002 *Plasma Sources Sci. Technol.* **11** 273
[132] Tynan G R, Burin M J, Holland C, Antar G and Diamond P H 2004 *Plasma Phys. Control. Fusion* **46** A373
[133] Shinohara S and Tanikawa T 2004 *Rev. Sci. Instrum.* **75** 1941
[134] Shinohara S and Tanikawa T 2005 *Phys. Plasmas* **12** 44502
[135] Motomura T, Shinohara S, Tanikawa T and Shamrai K P 2012 *Phys. Plasmas* **19** 043504

[136] Matsushita J, Sasaki K and Kadota K 1997 *Japan. J. Appl Phys. 1* **36** 4747
[137] Shinohara S, Tsuji H, Yoshinaka T and Kawai Y 1999 *Surf. Coat. Technol.* **112** 20
[138] Chen R T S, Breun R A, Gross S, Hershkowitz N, Hsieh M K J and Jacobs J 1995 *Plasma Sources Sci. Technol.* **4** 337
[139] Lynn A G, Gilmore M, Watts C, Herrea J, Kelly R, Xie S, Yan L and Zhang Y 2009 *Rev. Sci. Instrum.* **80** 103501
[140] Chang-Diaz F R 2006 *Thin Solid Films* **506–507** 449
[141] Boswell R W *et al* 2004 *Phys. Plasmas* **11** 5125
[142] Squire J P, Chang-Diaz F R, Glover T W, Jacobson V T, McCaskill G E, Winter D S, Baity F W, Carter M D and Goulding R H 2006 *Thin Solid Films* **506** 579
[143] Winglee R, Ziemba T, Giersch Prager L J, Carscadden J and Roberson B R 2007 *Phys. Plasmas* **14** 063501
[144] Prager J, Winglee R, Ziemba T and Roberson B R 2008 *Plasma Sources Sci. Technol.* **17** 025003
[145] Shamrai K P, Pavlenko V P and Taranov V B 1997 *Plasma Phys. Control. Fusion* **39** 505
[146] Carter C and Khachan J 1999 *Plasma Sources Sci. Technol.* **8** 432
[147] Charles C 1993 *J. Vac. Sci. Technol.* A **11** 157
[148] wikipedia.org
[149] Loewenhardt P K, Blackwell B D, Boswell R W, Conway G D and Hamberger S M 1991 *Phys. Rev. Lett.* **67** 2792
[150] Sakawa Y, Ohshima M, Ohta Y and Shoji T 2004 *Phys. Plasmas* **11** 311
[151] Benjamin N, Chapman B and Boswell R 1991 *Proc. SPIE* **1392** 95
[152] Tepermeister I, Blayo N, Klemens F P, Ibbotson D E, Gottscho R A and Lee J T C 1994 *J. Vac. Sci. Technol.* B **12** 2310
[153] Tepermeister I, Ibbotson D E, Lee J T C and Sawin H H 1994 *J. Vac. Sci. Technol.* B **12** 2322
[154] Gibson G W Jr, Sawin H H, Tepermeister I, Ibbotson D E and Lee J T C 1994 *J. Vac. Sci. Technol.* B **12** 2333
[155] Tynan G R *et al* 1997 *J. Vac. Sci. Technol.* A **15** 2885
[156] Chen F F, Evans J D and Tynan G R 2001 *Plasma Sources Sci. Technol.* **10** 236
[157] Chen F F, Jiang X and Evans J D 2000 *J. Vac. Sci. Technol.* A **18** 2108
[158] Yano M and Walker M L R 2006 *Phys. Plasmas* **13** 063501 and **14** 033510
[159] Chen F F 2014 Helicon source for ion propulsion *Encyclopedia of Plasma Technology* (New York: Taylor and Francis) submitted
[160] Chen F F 1984 *Introduction to Plasma Physics and Controlled Fusion* vol 1 *Plasma Physics* 2nd edn (New York: Plenum) p 293
[161] Charles C 2007 *Plasma Sources Sci. Technol.* **16** R1
[162] Chen F F 2006 *Phys. Plasmas* **13** 034502
[163] Hooper E B 1993 *J. Propul. Power* **9** 757
[164] Winglee R, Ziemba T, Giersch L, Prager J, Carscadden J and Roberson B R 2007 *Phys. Plasmas* **14** 063501
[165] Singh N, Rao S and Ranganath P 2013 *Phys. Plasmas* **20** 032111
[166] Merino M and Ahedo E 2014 *Plasma Sources Sci. Technol.* **23** 032001
[167] Lemmer K M, Gallimore A D and Smith T B 2009 *Plasma Sources Sci. Technol.* **18** 025019
[168] Takahashi K, Lafleur T, Charles C, Alexander P, Boswell R W, Perren M, Laine R, Pottenter S, Lappas V, Harle T and Lamprou D 2001 *Appl. Phys. Lett.* **98** 141503
[169] Chen F F and Curreli D 2013 *Phys. Plasmas* **20** 057102
[170] Chen F F and Torreblanca H 2007 *Plasma Phys. Control. Fusion* **49** A81
[171] Chen F F and Torreblanca H 2009 *Phys. Plasmas* **16** 057102